UNIVERSIDADE D
COIMBRA

Óscar Gabriel Bernardes Martins

MATLAB-Based Simulator For Radio Stripe Communications

Dissertation in the context of the Master's Degree in Electrical and Computer Engineering, Specialization in Telecommunications, Subspecialization in Mobile and Optical Communications and Networks and Services, supervised by Prof. Dr. Marco Alexandre Cravo Gomes and Prof. Dr. Vítor Manuel Mendes da Silva and presented to the Faculty of Sciences and Technology, Department of Electrical and Computer Engineering.

September 2022

MATLAB-based Simulator for Radio Stripe Communications

Supervisor:

Professor Doutor Marco Gomes

Co-Supervisor:

Professor Doutor Vítor Silva

Jury:

Professora Doutora Maria do Carmo Raposo de Medeiros

Professora Doutora Rita Cristina Girão Coelho da Silva

Professor Doutor Marco Alexandre Cravo Gomes

Dissertation submitted in partial fulfillment for the degree of Master of Science in Electrical and Computer Engineering.

Coimbra, September 2022

Acknowledgements

Em primeiro ligar, quero prestar um agradecimento aos meus orientadores, Doutor Marco Gomes e Doutor Vítor Silva, pela ajuda e motivação que proporcionaram durante o desenrolar desta dissertação, mas também ao professor Rui Dinis pelas suas sugestões.

Seguidamente, agradeço ao DEEC/UC e ao Instituto de Telecomunicações pela oportunidade concedida e por todas as condições fornecidas. Agradeço também a todos os colegas de curso que ao longo do mesmo estudaram e trabalharam ao meu lado. Aos compinchas do IT, por todas as pausas e cafés para desanuviar do trabalho. Um obrigado especial ao João e ao Filipe por estarem sempre dispostos a ajudar e por aturarem os lançamentos ocasionais.

Ao NEEEC/AAC, do qual fiz minha sala de trabalho durante um ano, e aos que nela conviveram comigo. Às comissões organizadoras da 6ª e 7ª edição do Bot Olympics, em especial ao Luís e à Marta, que apesar de todo o trabalho que deram, proporcionarem-me dos melhores momentos e recordações do curso.

Aos amigos que este curso me trouxe e que fizeram com que estes anos se passassem mais rápido: ao Cavaleiro, Baltazar, Miguel e Simão. Em especial, quero agradecer ao Diogo, por ser um excelente companheiro de trabalho e um ainda melhor amigo. Por todo o apoio que me deste, preocupação que demonstraste e pelas crises existenciais em solidariedade comigo. (E claro, por todos os memes e stickers).

Um agradecimento especial aos meus pais e às minhas irmãs, por esta oportunidade, por confiarem nas minhas capacidades e por todo apoio fornecido que me permitiu chegar onde estou.

Por fim, quero agradecer à Carolina, por todo o apoio que me deu e por nunca me ter deixado desistir. Por ter suportado todas as dores de cabeça que lhe dei, por me fazer companhia até às tantas da madrugada a trabalhar e por toda a preocupação comigo. Obrigado por fazeres de mim uma pessoa melhor.

A todos aqueles que influenciaram o meu percurso académico,

Muito Obrigado!

Este trabalho é financiado pela FCT/MEC através de fundos nacionais e quando aplicável cofinanciado pelo FEDER, no âmbito do Acordo de Parceria PT2020 no âmbito do projeto UIDB/50008/2020, UIDP/50008/2020.

Abstract

In the last decade, wireless communications have suffered a paradigm shift with the appearance of the 5^{th}–generation (5G) and, the already envisioned, beyond 5G networks. The improvements brought by this cellular generation do not limit themselves to increasing data throughput, having numerous other advantages, such as low latency and error rates, allowing the implementation of new technologies with critical communications needs throughout multiple fields.

Proper beyond 5G design presents a wide variety of challenges, requiring new concepts and technologies to be brought forth. Massive MIMO (mMIMO) and Cell-Free (CF) mMIMO systems are some of the new concepts used, focusing on increasing the number of Access Points (APs) in a distributed manner, providing higher Spectral Efficiency (SE) and uniform coverage. Practical deployments can be achieved using Radio Stripe (RS), which raises special interest due to its practicality, ease of installation, and low energy requirements. Nonetheless, to achieve fully operational deployments, the study of the RS transmission channel is essential. To such end, a mathematical model for uplink transmission under Line-of-sight (LOS) conditions was developed and used to study the system performance under several characteristics important to its design.

In the absence of interference, system performance was shown to increase logarithmically with the stripe length and to decrease inversely with the distance between the User Equipments (UEs) and the stripe. However, the highest detrimental factor to it has shown to be an unfavorable (large) Angle of Arrival (AoA). In multiuser scenarios, UEs interference was detrimental in proximity to the stripe, especially in small RSs. However, this can be reduced by operating at Millimeter-Wave (mmWave) frequency bands compared to sub-6 GHz bands. While excessively increasing the RS length does not provide any direct improvement to SE, it allows for optimised segmentation and service APs allocation.

Keywords: Radio Stripe, Multiple-Input Multiple-Output (MIMO), Cell-Free (CF) mMIMO, Millimeter-Wave (mmWave) Communications

Resumo

Na última década, as comunicações sem fios sofreram uma mudança de paradigma com o aparecimento das redes de quinta geração (5Gs) e, as envisionadas, pós-5Gs. As melhorias introduzidas por esta geração não estão limitadas a aumentos da taxa de transferência de dados, havendo inúmeras outras vantagens, tais como baixa latência e taxa de erro, que permitem a implementação de novas tecnologias com necessidades de comunicações críticas.

Uma implementação adequada de redes pós-5G apresenta uma grande variedade de desafios, exigindo que novos conceitos e tecnologias sejam postos em prática. Os sistemas Massive MIMO (mMIMO) e Cell-Free (CF) mMIMO são alguns dos novos conceitos utilizados, focando-se no aumento do número de pontos de acesso (APs) de forma distribuída de modo a proporcionar uma maior eficiência espetral e cobertura uniforme. Implementações destes conceitos podem ser conseguidas através da utilização de Fitas de Rádio (RSs), que suscitam um interesse especial devido à sua facilidade de instalação e baixo custo, e consumo energético. No entanto, de modo a projetar sistemas completamente operacionais, o estudo do canal de transmissão de RSs é essencial. Com esse fim, um modelo matemático para a transmissão em linha de vista foi desenvolvido. Este foi utilizado para estudar o desempenho do sistema tendo em conta diversas características importantes na projeção do mesmo.

Na ausência de interferência, o desempenho do sistema aumenta logaritmicamente com o comprimento da fita e decresce inversamente com a distância entre os equipamentos terminais (UEs) e a mesma. Os ângulos de chegada tangentes revelaram-se o fator mais prejudicial para o desempenho. Em cenários com múltiplos utilizadores, a interferência entre os mesmos mostrou degradar o funcionamento do sistema nas imediações da fita, especialmente para RSs com tamanhos inferiores à área abrangida pelos UEs. Sistemas a operar nas bandas de frequências de ondas milimétricas (mmWaves) mostraram-se ser mais resilientes à interferência do que os que operaram em bandas inferiores a 6 GHz. Aumentar excessivamente o comprimento em relação à área abrangida pelos UEs não proporciona melhorias à eficiência espetral. Porém, permite a otimização da segmentação e alocação de APs a servirem os UEs.

Palavras-Chave: Fita de Rádio, múltiplas entradas e múltiplas saídas (mMIMO), *Cell-Free* (CF) *Massive MIMO* (mMIMO), ondas milimétricas.

"Now I'm a scientific expert; that means I know nothing about absolutely everything."

— Arthur C. Clarke

"The greater danger for most of us is not that our aim is too high and we miss it, but that it is too low and we reach it."

— Michelangelo

Contents

List of Acronyms

1G	1^{st}-generation
5G	5^{th}–generation
AoA	Angle of Arrival
AP	Access Point
APU	Antenna Processing Unit
AWGN	Additive White Gaussian Noise
BS	Base Station
CF	Cell-Free
CSI	Channel State Information
CPU	Central Processing Unit
CDM	Code-Division Multiplexing
CDMA	Code-Division Multiple Access
DL	Downlink
EE	Energy Efficiency
eMBB	enhanced Mobile Broadband
FSPL	Free-Space Path Loss
FDD	Frequency-Division Duplex
FDM	Frequency-Division Multiplexing

FDMA	Frequency-Division Multiple Access
IRS	Intelligent Reflective Surfaces
LIS	Large Intelligent Surface
LOS	Line-of-sight
LiFi	Light Fidelity
MF	Matched Filter
MIMO	Multiple-Input Multiple-Output
MISO	Multiple-Input Single-Output
mMIMO	Massive MIMO
MMSE	Minimum Mean-Square Error
mmWave	Millimeter-Wave
MU-MIMO	Multi-User MIMO
NLOS	Non-line-of-sight
OWC	Optical Wireless Communications
RF	Radio Frequency
RIS	Reconfigurable Intelligent Surface
RS	Radio Stripe
SC	Small-Cell
SD	Spatial Diversity
SDMA	Spatial Division Multiplexing Access
SM	Spatial Multiplexing
SE	Spectral Efficiency
SNR	Signal-to-Noise Ratio
SINR	Signal-to-Interference-plus-Noise Ratio

SISO	Single-Input Single-Output
SIMO	Single-Input Multiple-Output
TDD	Time-Division Duplex
TDM	Time-Division Multiplexing
TDMA	Time-Division Multiple Access
UE	User Equipment
UL	Uplink
VLC	Visible Light Communications
ZF	Zero-Forcing

List of Figures

List of Tables

Notation

Mathematical notations are listed below in the respective order:

$\mathbf{A^H}$	conjugate-transpose matrix
$\mathbf{A}^*$	complex conjugate matrix
$\mathbf{A^{-1}}$	inverse matrix
$\mathbf{a_{m,n}}$	the matrix element in m^{th} row and n^{th} column
$\mathbf{a_m}$	the m^{th} vector
$\star$	linear convolution
E $(\cdot)$	Mathematical expectation / mean value

Matrices and vectors are denoted with boldface letters.

1 Introduction

In the middle of the twentieth century, the world entered the Information Age with the appearance of transistors, optical amplifiers and fibers, and bases of computation. Information Technologies shifted to be the central part of our society, affecting everything from economics to culture, and with each passing day data gains new uses and a higher value [1]. Telecommunications have since become a backbone of society. While initially only wired communications prevailed, it was in the 1980s that the first commercial mobile communications systems started to appear together with the concept of dividing the coverage area into cells, creating the 1^{st}-generation (1G) of cellular networks. Since then, these networks have evolved a lot, with each new generation being a major paradigm shift that has broken backward compatibility [2]. The last one, the 5^{th}–generation (5G), has allowed various new applications such as Virtual and Augmented Reality, HD screening, video conferencing and 360^{o} video streaming [3].

Cellular phone companies and communication providers started to deploy their versions of the 5G communication standard for broadband cellular networks in 2019. Although the impact of the improvements brought by 5G may not be very noticeable for standard network users, as they will most benefit from an increase in the data transmission speed in rate-centric enhanced Mobile Broadband (eMBB), this new wave in mobile communications brings numerous advantages, allowing the implementation of new technologies throughout multiple fields such as vehicular automation, medical robotics, and other services with critical communications needs.

Proper implementation of 5G presents a wide variety of challenges, requiring new concepts and technologies to be brought forth. A major one is to increase data throughput in wireless networks, which can be done in three ways: increasing the amount of spectrum used; obtaining better spectrum efficiency; and lastly, having a higher AP density. By the nature of such communication channels, throughput can't be increased simply by adding more transmission resources as in wired communications. The wireless medium cannot be physically

separated in the same location, meaning its associated spectrum is limited. To worsen this problem, not all frequencies are appropriate for information transmission, severely restricting spectrum usage. New 5G technologies are focusing on mmWave communications, using an unused part of the spectrum, which allows for faster networks, at the cost of having a more limited transmission range. Novel multiple access technologies, channel coding schemes, and waveforms are being studied in order to improve spectral efficiency [4].

Multiple-Input Multiple-Output (MIMO) and Massive MIMO (mMIMO) systems provide answers to increasing the amount of AP, by using multiple antennas at both the receiver and transmitter to achieve significant improvements in both data transmission and reliability compared to normal Single-Input Single-Output (SISO) systems. MIMO systems allow for either the enhancement of system reliability through spatial diversity [5] or increasing data transmission using spatial multiplexing [6]. It is also possible to achieve both gains by assuring a trade-off between them [7].

By increasing AP density and using higher transmission frequencies, i.e. mmWave, the cellular communications paradigm has started to change to accommodate Small-Cell (SC) topologies. Smaller cells, allow for an increase in the throughput for each user since a lower number of UE is expected to be served in each cell. Another current technology is Cell-Free (CF) mMIMO systems, which, as stated by their name, imply a system comprised of a large number of distributed, low cost and power APs antennas, connected to a network controller. This way, the coverage area is not partitioned into cells and each user is served by all APs simultaneously [8].

Fully functional implementations based on the referred technologies are yet to be available, but several new concepts show potential. Reconfigurable Intelligent Surfaces (RISs) and Large Intelligent Surfaces (LISs) [9], also known as Intelligent Reflective Surfaces (IRS) [10], are prominent examples. These consist of arrays of reflecting elements for reconfiguring the incident signals [11] and, in the case of LISs, signal processing capabilities. Radio Stripes (RSs) [12] are an antenna arrangement for distributed mMIMO, working similarly to a RIS, and are meant to be a low-cost, low-maintenance, easy-to-deploy, and non-intrusive solution to achieve cell-free uniform networks.

1.1 Motivation and Objectives

New envisioned technologies such as LISs, RISs, and RS can achieve higher spectral and power efficiency, and uniform coverage with high reliability. Although actual and fully oper-

ational implementations of these are scarce, or even nonexistent, some have been designed. Among these, RSs raise special interest due to their versatility, showing promise for being applied in large spaces where a single normal AP, or even a few spread ones, can't properly serve all expected users with uniform performance. While the installation is simple, an almost *plug & play* process, the layout of these stripes still requires correct and well-executed planning. In addition, although adding more antennas should always deliver better performance, it has an associated cost that should be avoided when it outperforms the benefits.

The goal of this thesis is to model and understand the transmission channel for RS usage, mostly under LOS conditions. To such end, RS will be described as a one-dimensional LIS and evaluated both as a continuous surface and as a discrete one. The behavior will then be analyzed based on the channel capacity and studied in function of the transmission wavelength, UE density, position and distance to the APs, and length of the RS in scenarios with interference and without it, i.e. multiple and single-user cases.

1.2 Dissertation Outline

This first chapter has provided a brief introduction to the state of communications focusing on wireless communications, new technologies, and implementations in the field, in order to provide a background and motivation for this thesis.

The remaining dissertation is divided into 5 chapters, organized in the following way:

Chapter 2

This chapter starts by presenting wireless communications. Initially, an overview of antenna technology and basic works is given, followed by wireless transmission and communications concepts, such as propagation and interference. Lastly, millimeter wave communication, its uses and setbacks are introduced.

Chapter 3

Here MIMO systems and their evolutionary categories, including Massive MIMO (mMIMO), are presented together with their benefits and setbacks. An overview of Cell-Free (CF) mMIMO deployments is also given.

Chapter 4

Radio Stripes (RSs) will be presented in this chapter, followed by the description and definition of a communication model for them, based on LOS propagation in both single and multi-user cases.

Chapter 5

This chapter presents the performance results, with average channel capacity as a metric, for the simulation of the RS model behavior . Firstly, an analysis of single-user behavior and array gain, are presented, focusing on the effects of array length, and UE's position and distance to the array. Afterward, the multi-user case study will be presented, focusing on two scenarios: large arrays, where their size overreaches the UE, and small arrays, where the array size is either the same or smaller than the space covered by the UE.

Chapter 6

This chapter concludes and summarises the results of this thesis and presents some future research lines.

2 Wireless Communications

This chapter introduces wireless communications and transmission focusing on some important issues such as propagation effects, interference, and the basics of wireless channel modeling.

2.1 Wireless Channel

Information transmission always requires an appropriate medium, which usually divides communications into two types: wired and wireless, with different requirements and advantages.

Wired communications use a guided transmission line and tend to be very reliable, suffering from low interference. As the available spectrum is very large and separated between different physical connections, data throughput can be easily increased by adding more of these. The biggest setback is the lack of mobility and flexibility that it provides to end users. Thus, they tend to be used the most in core and transportation networks.

On the other hand, in wireless communications, no physical connection for users is required, providing better mobility and easier access. Thus, making them more useful for the user in access networks.

Unfortunately, reliability and service quality are worsened due to a lot of aspects. Obstruction and environmental effects, such as rain and humidity, cause signals to reflect and refract, resulting in attenuation. Interference highly impacts these systems as the medium is not isolated between users. For this reason, several security concerns are also raised.

A major problem in wireless networks happens due to the medium being shared and unable to be expanded, which results in the spectrum becoming limited and with very restricted usage. Thus, scaling networks and increasing wireless throughput becomes a complex task.

High mobility, due to the lack of a physical connection, is the main advantage of wireless communications but induces the channel to become time and space-variant. Therefore, constant channel analysis is needed to ensure proper transmissions. This becomes especially

important in mobile communications, where these variations due to user movement are expected to happen frequently.

2.1.1 Antennas

Not all wireless communication systems use Radio Frequency (RF) technology. Optical Wireless Communications (OWC), Visible Light Communications (VLC), and Light Fidelity (LiFi) systems, use light sources like LEDs or fluorescent lights to transmit digitally modulated light and photo-detectors to receive it [13]. However, the more well-known and widely used systems do. These make use of a transitional structure between free space and a guiding device that emits and gathers energy in the form of electromagnetic waves using electrical conductors, known as antennas [14].

When sending a signal, the antenna transforms the radio-frequency electrical energy from the transmitter into electromagnetic energy, which is then radiated into the environment as a wave. When receiving a signal, the antenna is affected by the electromagnetic energy of the wave and converts it into radio-frequency electrical energy, feeding it to the receiver. The processes of transmitting and receiving a signal are then the opposite of each other. However, as long as the same frequency is employed, the same antenna can be used in both directions because their efficiencies are the same in both operations. [14]

Radiating Patterns

Radiating electromagnetic energy is the primary role of an antenna. Therefore, it makes sense to characterize its performance through a mathematical or graphical representation of its radiation properties as a function of the space coordinates. This representation is called a radiation pattern, or antenna pattern, and provides a convenient means of determining the beam width of an antenna. This is a common measure of the relative antenna gain in each direction or Directivity, i.e. "the ratio of the radiation intensity in a given direction from the antenna to the radiation intensity averaged over all directions" [15]. It is also noteworthy to state that there are no differences between receiving and radiating power, thus, it can also be known as receiving pattern.

There are two categories of antennas based on their radiating pattern. The simplest one produces an idealized antenna known as the isotropic antenna, defined as “a hypothetical lossless antenna having equal radiation in all directions" [16], originating a radiating pattern, presented in figure 2.1a , with a sphere centered around the antenna. The other one is the

directional antenna which delivers a preferred radiating direction along one axis, as seen in the radiation pattern lobes in figure 2.1b [14]. Note that, while isotropic antennas are purely theoretical radiators there are omnidirectional antennas, which have an essentially non-directional pattern in a given plane (figure 2.2), delivering close approximations to it [16].

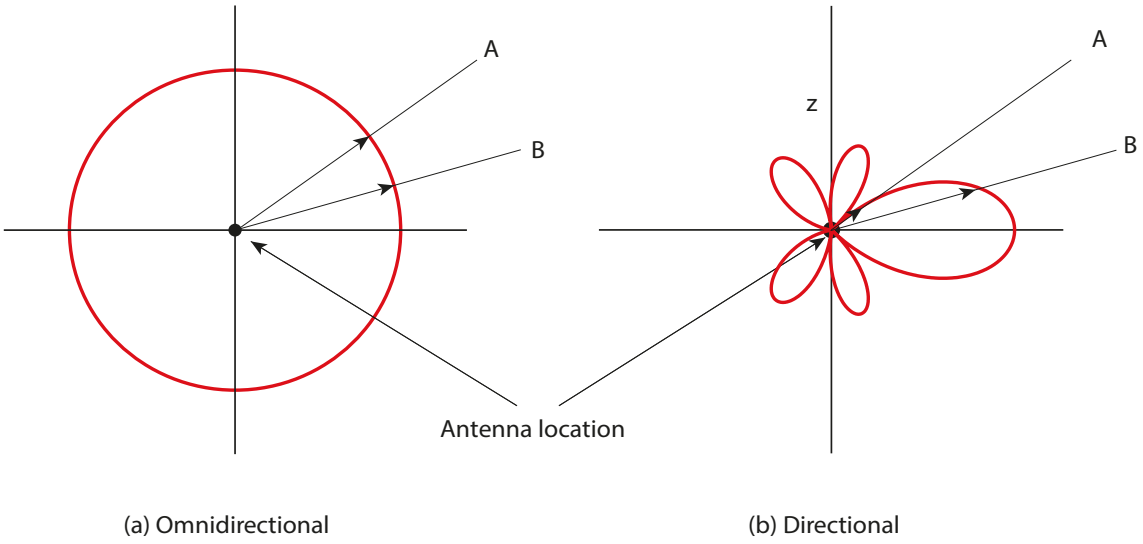

Figure 2.1: Antenna Patterns (from [14]).

Antenna Gains

Antennas come in various types, each holding different characteristics which allow for better performance in specific scenarios. Some of these have already been mentioned, such as the antenna pattern and directivity. Another important characteristic is the antenna gain, which is also a measure of directionality [14] and expresses the radiation intensity in a particular direction as a ratio to the power output of an isotropic radiator [15]. The antenna gain is a good indicator for describing the behavior of an antenna. For this reason, this metric tends to be commonly used when studying wireless communication channels.

For an antenna to have a more significant gain in a given direction, it comes at the expense of other directions, i.e., increasing radiated power in a direction reduces power in others. It is important to note that this gain does not refer to obtaining more output power than input power but rather to directionality. Antenna gain is related and dependent on another characteristic, the effective area of an antenna. This area, or aperture, is the surface of a plane near the antenna where most of the harvested energy passes. This is related to

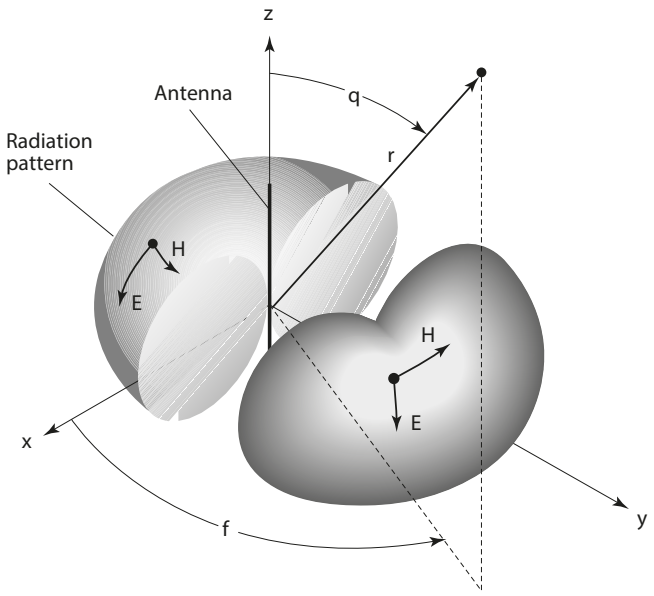

Figure 2.2: Antenna Pattern of an omnidirectional antenna (from [16]).

the physical size of the antenna and its shape, thus different antennas end up with different effective areas and different gains, as presented in table 2.1. Therefore, the antenna gain (G) is given as

$$G = \frac{4\pi A_e}{\lambda^2} = \frac{4\pi f^2 A_e}{c^2} \ , \tag{2.1}$$

where A_e is the effective area, f is the carrier frequency, c is the speed of light (3×10^8 m/s) and λ is the carrier wavelength.

Since the gain is also dependent on the carrier wavelength, an antenna would only perform equally at both receiving and radiating energy if the communications are done at the same frequency and medium, as previously mentioned.

Antenna Arrays

While there are many scenarios when only one antenna of a given type is needed, it is quite common to have a certain access point with many antennas. These antennas can work in cooperation in both transmission and reception, giving rise to various types of wireless communications, such as Single-Input Multiple-Output (SIMO), Multiple-Input Single-Output (MISO) and MIMO. The advantage of using an array of antennas instead of a single antenna is that these multiple antennas can be configured to produce a directional beam. By adjusting their impedance, or complex weights, z_k, which can be optimized for different criteria, phases, amplitudes, and time delays may be altered and an overall sum of antenna patterns with a preferred directivity in a chosen direction may be obtained [14].

Table 2.1: Antenna Gains and Effective Areas (from [14]).

Type of Antenna	**Effective Area A_e (m^2)**	**Power Gain (relative to isotropic)**
Isotropic	$\lambda^2/4\pi$	1
Infinitesimal dipole or loop	$1.5\lambda^2/4\pi$	1.5
Half-wave dipole	$1.64\lambda^2/4\pi$	1.64
Horn, mouth area A	0.81A	$10A/\lambda^2$
Parabolic, face area A	0.56A	$7A/\lambda^2$
Turnstile (two crossed, perpendicular dipoles)	$1.15\lambda^2/4\pi$	1.15

The radiation from the electric field produced by an array of N antennas is given by

$$E = \mathrm{Re}\left[E_0 \exp(j\omega t) \sum_{k=1}^{N} z_k \frac{1}{d_k} \exp\left(-\frac{j2\pi d_k}{\lambda}\right)\right] \tag{2.2}$$

where d_k is the distance from any given antenna k in the array to the receiver.

Despite being in use for many years, directional antennas are becoming increasingly practical and useful in modern communication systems. In cellular communications, sets of directional antennas in a triangular configuration of antennas are used to achieve a split of the coverage area into three 120^{o} sectors. In modern applications, adaptive antenna arrays [17], are dynamically configured to follow individuals or groups of users, allowing the service to focus on their specific location with strong gains.

Near and Far-Fields Regions

The space surrounding an antenna is usually divided into various regions with different field structures. Generally, three sub-divisions are brought up: reactive near-field, radiating near-field, and far-field which are separated by boundaries defined by established criteria (see figure 2.3). While these boundaries divide regions with different field configurations, they do not present abrupt changes [16].

What characterizes these field regions is the behavior of the magnetic (**H**) and electric (**E**) fields concerning each other. To have propagation fields, the **E**/**H** fields must be orthogonal and in-phase. However, in the reactive near-field, the closest to the antenna, they are 90^{o} out of phase, thus making them reactive. In the radiating near-field, they start to transition

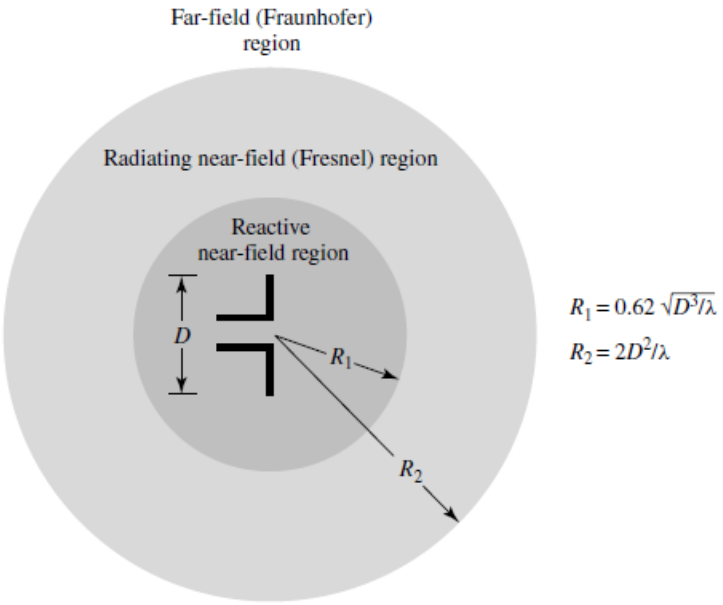

Figure 2.3: Field Regions of an antenna (adapted from [16]).

to being radiating, i.e. getting in phase, achieving it in the far-field. Afterward, while they do die off as the distance to the antenna increases, they do not suffer changes in their shape.

The size of these field regions and respective boundaries are dependent on the maximum overall dimension of the antenna, D, and the propagation wavelength. When D is large compared to the wavelength, $D > \lambda$, the first region exists when the distance to the antenna, R, is

$$R < 0.62\sqrt{D^3/\lambda} \quad , \tag{2.3}$$

after which we have the radiating near-field that will last until the far-field starts, at

$$R > 2D^2/\lambda \quad . \tag{2.4}$$

These two boundaries and respective regions are usually known as the Fresnel and Fraunhofer distances/regions respectively, based on analogy to optical terminology [16]. It's also important to note that the intermediate region, the radiating near-field, may not exist under the circumstance where the maximum overall dimension of the antenna is negligible compared to the wavelength, i.e. $D << \lambda$ [16].

It's worthy of note that, when antenna arrays are used, we can be in presence of a scenario where the communication between the UE and each antenna happens in the far field, and so no reactive components need to be taken into consideration, but at the same time, it might be in either the reactive or radiating near-field of the array. This means that while there are

no differences between the propagating wave that reaches distinct parts of the same antenna element, there might be differences between the wave at each antenna element of the array. This becomes more common as LIS, RIS, or any other type of Physically Large Antenna Arrays, where the near-fields are far-reaching, become more popular.

2.1.2 Propagation

The propagation of a transmitted signal is the basis of the analysis and estimation of the wireless communication channel and it depends on a lot of factors, such as distance, environment, object presence, LOS conditions, and even terminal movement. During wireless transmission (figure 2.4), the electromagnetic waves which transmit information can be damped, suffer diffusion/scattering, be reflected, and suffer temporal dispersion. All these factors combined lead to large-scale (or slow) fading, like path loss (P) and shadowing (S), which originated over distances of several tens of wavelengths, and small-scale (or fast) fading effects appearing as a result of multi-path propagation (M), observed over a distance of the order of the wavelength [18]. In addition, while not specific to wireless communications, the transmitted signal will always be subject to unwanted signals referred to as noise.

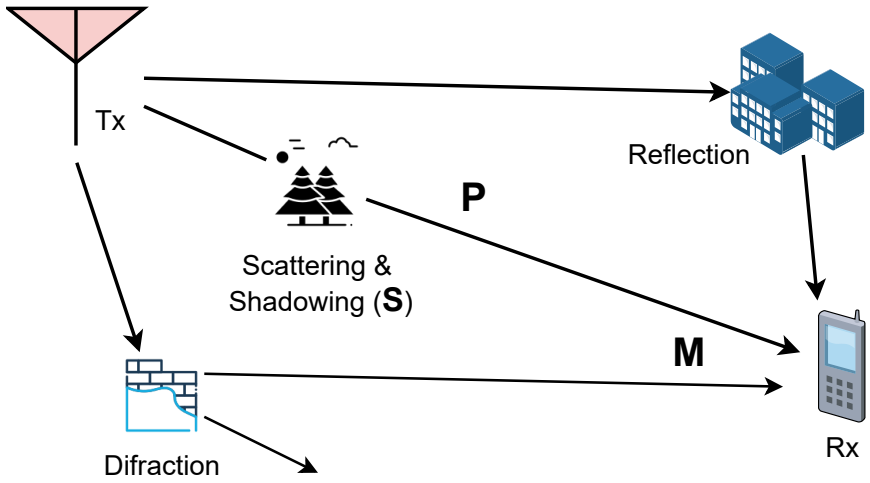

Figure 2.4: The appearance of large and small-scale fading in the propagation of wireless communication.

Path loss

Path loss, P, is the power loss or attenuation which the transmitted signal suffers while propagating in LOS conditions through the channel **h**. This attenuation between the transmitter (Tx) and the receiver (Rx) is normally modeled by the Friis transmission equation [19] for

free-space propagation, or Free-Space Path Loss (FSPL), in which the power at the receiver (P_r) at a distance, d, is given in reference to the power at the transmitter (P_t) such that

$$\frac{P_r}{P_t} = G_r G_t \left(\frac{\lambda}{4\pi d}\right)^2, \tag{2.5}$$

where λ is the carrier wavelength, that can be expressed in terms of the carrier frequency, f, and the light speed of propagation in vacuum, c, as $\lambda = c/f$, while G_t and G_r represent the transmitter and receiver antennas gains, respectively, and are given by (2.1). Thus, for generic antennas the FSPL is expressed as

$$\frac{P_r}{P_t} = \frac{A_r A_t}{(\lambda d)^2} \quad . \tag{2.6}$$

as a function of the effective areas of the receptor and transmitter antennas, A_r and A_t.

Thus, based on the previous equation, the attenuation between the two antennas increases with the square of the distance in which the signal must transverse. Equation (2.5) shows that FSPL increases with the square of wavelength, meaning higher carrier frequencies result in higher free-space attenuation.

In reality, while its behavior generally keeps true to what was previously mentioned, attenuation is not as linear and systematic. Wireless electromagnetic signals in real environments suffer from atmospheric absorption, which varies non-linearly with the carrier frequency as shown in figure 2.5, or other obstructions. This results in higher attenuation than in free space [18] being observed in experiments for different path loss models, such as Okumura-Hata, Lee Propagation, and COST Hata models. One of such models [20], albeit a simplistic one, describes path loss as

$$L = 10n \log_{10}\left(\frac{d}{d_{ref}}\right) + L_{ref} \quad [dB]\,, \tag{2.7}$$

where n is the path loss exponent and L_{ref} is the reference attenuation for the distance d_{ref}, which might be based on (2.5) or slightly different depending on the antennas used. As the exponent is conditional to the level of obstruction of the environment, ranging from 2 (free space) to 6 (severe obstruction), it allows for a better representation over simply applying (2.5) [21].

Shadowing

The presence of obstacles between the transmitter and the receiver causes absorption, reflection, scattering, and diffraction. It also results in attenuation effects known as shadowing (or

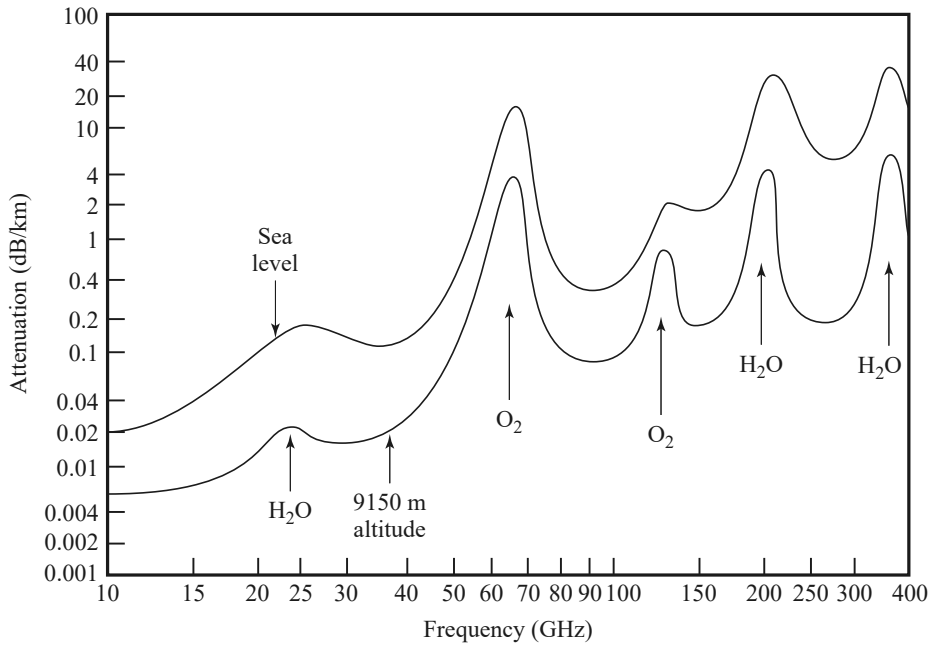

Figure 2.5: Atmospheric absorption (dB/Km) as a function of the communication carrier frequency (from [22]).

shadow fading) (S). So at two places at any given distance, d, from the transmitter and with similar path loss conditions, different attenuation losses can be verified due to objects in the signal path. The total power loss is the result of the product of the power loss originated by each object in the path of the signal, which is equivalent to the sum of the losses in the log domain. The total loss would then become

$$L = 10n \log_{10}\left(\frac{d}{d_{ref}}\right) + L_{ref} + S \quad [dB]\,, \tag{2.8}$$

where S represents the shadowing effect in dB. Based on the central limit theorem, this shadowing has a normal or Gaussian distribution in the log domain and so, it can be modeled as a log-normal distribution.

Multipath Fading

Other than large-scale fading, path loss, and shadowing, wireless communications also suffer from small-scale (or fast) fading effects, as a result of Non-line-of-sight (NLOS) conditions which are very common in urban networks.

Multipath propagation occurs when a signal reaches the receiver from two or more different paths. This can happen due to local scatters, such as mountains or buildings, which obstruct the LOS between the Tx and Rx, which reflect or diffract the original signal. In

other words, new NLOS propagation paths appear, resulting in signals with different delays and angles, phase and frequency shifts (i.e. Doppler Effect), and attenuations appear, with variations that can reach up to 40 dB in one half-wavelength, which will vectorially combine at the receiver antenna to produce a composite received signal. This combination can be constructive or destructive and is known as multipath fading [21].

In environments that give rise to NLOS scenarios, propagation is mostly modeled using statistical fading models which assume the reception of an infinite number of independent signals. These impinge on the receiver from different directions, usually described as phase shifts. Different models describe environments and propagation paths with various characteristics. Rayleigh-distributed fading models described an environment where all paths are obstructed to a certain degree, while Rician-distributed fading models consider scenarios where there is a path with a stronger signal component, namely a LOS path [20].

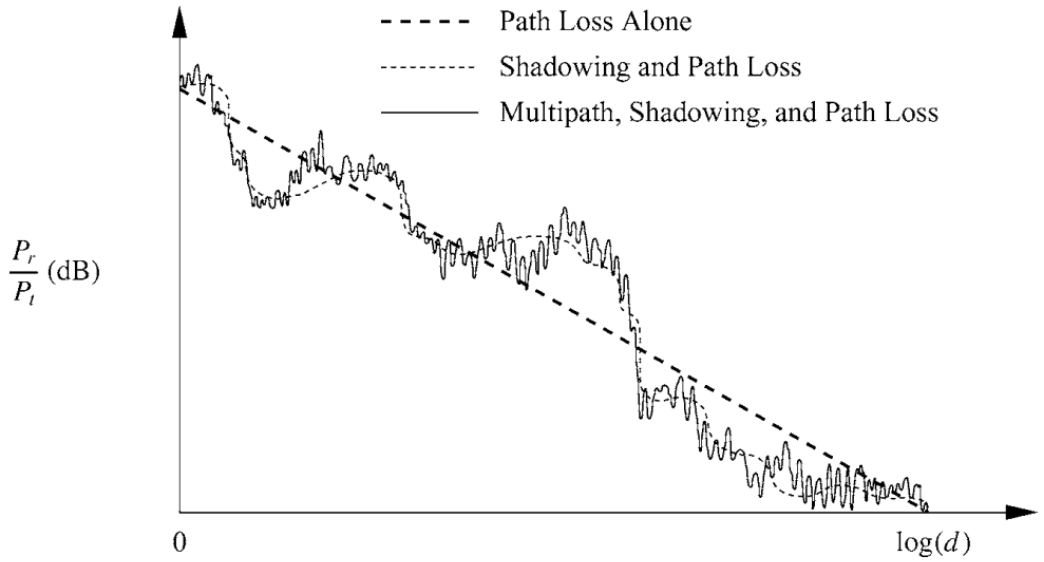

Figure 2.6: Effect of path loss, shadowing, and multipath fading in propagation as a function of the distance between Tx and Rx (from [23]).

Noise

In any transmission, the received signal will consist of the transmitted signal, affected by its channel effects, such as attenuation and phase shifts or delay, plus additional unwanted signals. These unwanted signals are known as noise and are a major limiting factor in communications system performance. Their effects can vary depending on the end product of the transmission, be it hiss or buzzing in audio format or flicker and color "pepper spray"

in video and image formats. Still, overall they create errors in the transmitted data that the system might not be able to correct.

Noise can be produced by several effects and is denominated and treated differently based on that. Some are unique to a specific type of communication or technology, while others are expected to happen in any transmission and can be modeled. A common division of noise into categories goes as follows: Thermal Noise, Intermodulation Noise, Cross Talk, and Impulse Noise.

Thermal Noise, also known as Electrical Noise, is a signal generated due to the thermal agitation of electrons in all electronic devices in the transmission media, and its intensity is related to the temperature of the device. Since its power remains the same along the frequency spectrum with equal intensity, i.e. it's uniformly distributed, it's commonly referred to as white noise. Given that it can not be eliminated, it acts as an upper bound for the performance of the communications systems.

For Thermal Noise, the noise power density in Watts per Hz of bandwidth, N_0, is given by

$$N_0 = kT \quad (\text{W/Hz}) \tag{2.9}$$

where, k is the Boltzmann constant and T is the absolute temperature in Kelvin. Since this noise is independent of the frequency, the total noise power is just a linear scaling based on the bandwidth.

Wireless communications shared medium is usually divided into different frequency regions to achieve simultaneous communications. The result of using multiple frequencies in the same medium is the appearance of intermodulation noise. Mixing signals with different frequencies might cause energy to be produced at multiples of the sum of their frequencies and interfere with an intended signal at such frequency. The actual appearance of this noise happens under circumstances of non-linearity in the transmitter, receiver, or other intervening transmission elements resulting from component malfunction, nature of the amplifiers, or excessive signal strength.

Cross talk noise is normally associated with wired communications, particularly when used in twisted pairs cabling or, rarely, with coaxial cabling, and happens due to electrical coupling between signals transmitted through the same lines. In wireless communications systems, it can happen when unwanted signals, typically at the same order of magnitude as thermal noise, are captured by the antenna. While this is unlikely, as highly directional antennas and medium access schemes are usually used, this type of noise tends to be the

dominant type in unlicensed ISM bands.

Lastly, there is impulse noise, which is the hardest to deal with due to its unpredictability and high magnitudes. It can be originated from various causes, including external electromagnetic disturbances, such as lightning, and faults and flaws in the communication system. While the duration of these impulses is relatively small for analog communications, for communications with high-speed data transfer, a single impulse is enough to generate thousands of bit errors in a simple 1 Mbps line. Therefore, it is the primary source of error in digital communications.

2.1.3 Multiuser Communication Systems

Amongst the multitude of factors that difficult optimization of wireless channel communications, a major one has yet to be introduced. Wireless communications operate with a broadcast nature, thus, an electromagnetic wave of a transmitted signal will not travel through a single preferred path and project its field into a single receiver antenna. Instead, the signal transmitted from a certain UE will affect all the surrounding antennas in its wave propagation radius. This behavior is the basis of the interference component in wireless communication channels.

Interference, from a certain perspective, can be regarded as cross-talk noise, i.e. unwanted electromagnetic signals captured at the receiver antenna. However, while cross-talk noise is normally uncontrollable, even if expected to a certain point, interference originating within the same communication system can be reduced by the combined means of power and medium access control.

Since the nature of the problem revolves around the existence of unwanted high-magnitude signals, reducing the interfering signal power at the source is a valid option. However, there are power limitations that need to be followed for communication to be possible, notably, the antenna receiving sensibility. Power optimization schemes can be used in wireless communication to maximize metrics regarding interference, namely the Signal-to-Interference-plus-Noise Ratio (SINR). However, techniques to limit simultaneous transmissions should be used foremost. To this end, medium access control schemes and signal multiplexing are typically used. These methods are divided into Time-Division Multiple Access (TDMA), Frequency-Division Multiple Access (FDMA), Code-Division Multiple Access (CDMA), and Spatial Division Multiplexing Access (SDMA), which control which devices can access and transmit to the medium; and Time-Division Multiplexing (TDM), Frequency-Division Mul-

tiplexing (FDM), Code-Division Multiplexing (CDM), and Spatial Multiplexing (SM) for allowing multiple signals to be combined and transmitted over a single medium. While perfect results can not be obtained, due to synchronization problems, non-ideal filters, and limits to beamforming, these methods help system performance by highly reducing interference.

2.2 Millimeter Wavelength Communications

The lower end of the electromagnetic spectrum, i.e. frequencies until 6 GHz, is mostly reserved for all types of wireless communication, such as radio broadcasting, aeronautical communication, and mobile networks. Common wireless systems make preferable use of frequencies of the 300MHz - 6 GHz range, known as sub-6 GHz bands, which allow for radio waves that can penetrate buildings, reflect multiple times, and bend around corners. The frequency range from 30 GHz to 300 GHz, usually referred to as the mmWaves band due to the wavelength ranging from 1 to 10 mm, is practically empty, as seen in figure 2.7. Frequencies in this band suffer from high atmospheric absorption, rain attenuation, high penetration and reflection losses, and low diffraction. These conditions highly limit its usage in wireless systems, restricting them only to be used in LOS outdoor-to-outdoor or indoor-to-indoor scenarios, and only over short distances. Nevertheless, since spectrum space is a valuable resource, exploration of this band has been a target for wireless communications [24].

Currently, the main use for mmWave communications is wireless backhaul in the unlicensed 60 GHz band, presenting a cost-effective solution compared to WLANs (based on the IEEE 802.11ad standards) and wired communications. For access networks, these communications perform the best in SC networks, i.e. a network where the coverage area of each base station is small, resulting in a lesser amount of users being served with higher spectral efficiencies. In these networks, mmWaves have been found to be viable when the transmitter and receivers are equipped with a sufficiently large antenna array to compensate for losses. This larger number of antennas is justifiable based on Friis' transmission formula for FSPL presented in (2.5) and its subsequent result in (2.6), where we can observe that, for a fixed FSPL, the effective areas have to scale with $A_t A_r \sim \lambda^2$. Since the antenna array's effective area will scale with the number of antennas, as long as this increase is sufficiently high enough, the path loss for mmWave communications can remain the same as for sub-6 GHz communication. This increase needs to be achieved in the whole the system, thus, in wireless mobile communications tends to be focused on the base station due to terminal limitations.

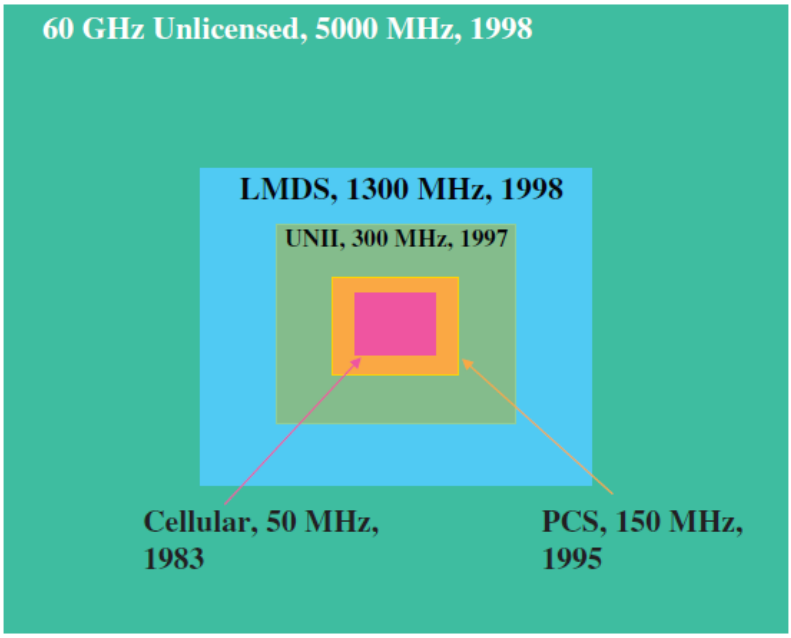

g

Figure 2.7: Available licensed and unlicensed spectrum bandwidths in popular UHF, microwave, 28 GHz LMDS, and 60 GHz mmWaves bands in the USA, illustrated through square areas (from [25]).

Björnson *et al.* (2017) [24] show that, under the assumption of the antenna effective area decreasing with the frequency, as in $A_e(\lambda) = 0.1252\lambda$, the number of half-wavelength dipoles that a wireless system needs to achieve the same FSPL grows linear with f_c/f_{co}, where f_{co} is the reference frequency and f_c the target frequency, as exemplified in figure 2.8 for $f_{co} = 3$ GHz. Since the transmission bandwidth usually increases in mmWave communications, the actual number of antennas required may grow if the same Signal-to-Noise Ratio (SNR) is expected to be kept. However, due to mmWave frequencies propagation characteristics, achieving the SINR at higher frequencies might be more doable than achieving the same SNR, since any transmitted signal is attenuated faster, which results in less interference.

Nevertheless, while mmWave communications can be used in both transport and access networks, some caveats are important to be aware of. Firstly, while antenna arrays allow for mmWaves to be used in wireless systems due to their high array gain, they require the narrow transmit and receive beams to be aligned. Thus, LOS obstructions highly degrade the system performance [26]. Secondly, it is extremely hard to have an RF chain for every radiating element in an array, especially in the user terminal due to cost, size, and energy requirements. This escalates further with mmWave, since power amplifiers and DACs / ADCs get very power-consuming when bandwidth is increased [27, 25]. Lastly, the coherence inter-

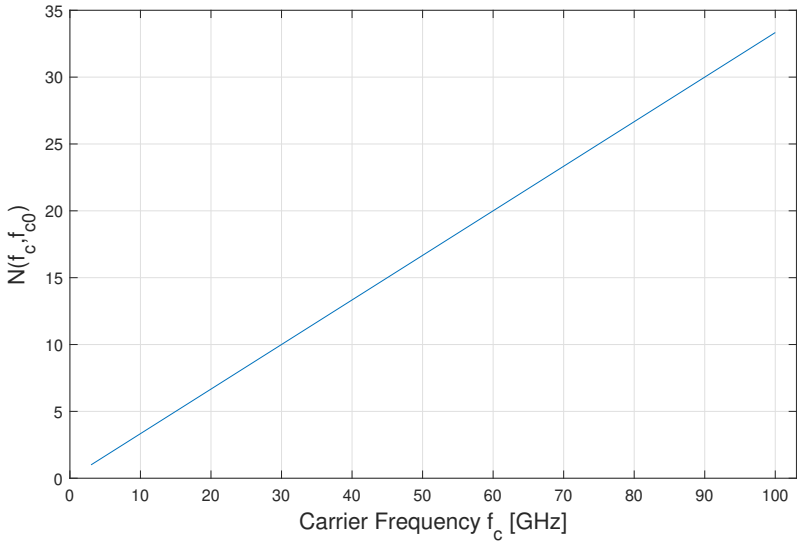

Figure 2.8: Function $N(f_c, f_{c0})$ shows how many times more antennas are needed at the system working at frequency f_c to obtain the same path loss as at frequency $f_{c0} = 3$ GHz (adapted from [24]).

val, or coherence block, i.e. the time-frequency space at which the communication channel is considered constant and flat-fading, has a duration that scales linearly with wavelength and inversely proportionally with delay spread [28]. Therefore, for mmWave communications, the coherence interval becomes too small and requires more frequent pilot signals than for sub-6 GHz band. Notice, however, that this can be counterbalanced since mmWaves access networks are expected to have small cell radius and serve user terminals with low mobility, resulting in a smaller delay spread [24].

All in all, mmWave communications seem to be best suited to SC or CF topologies, excelling in providing high throughputs to slow-moving user terminals. Later chapters in this thesis will study a CF topology at the Uplink (UL) scenario, comparing its performances at both sub-6 GHz and mmWave frequency bands.

3 MIMO Systems

In this chapter MIMO technology, and its different categories of MIMO will be presented, with a focus on Massive MIMO (mMIMO). The CF mMIMO deployments, their benefits, and practical issues will also be analyzed at the end of the chapter.

3.1 MIMO

The use of multiple antennas at the transmitter and receiver, known as MIMO technology, is a natural progression of development in antenna array communication. This has rapidly gained popularity over the past decades due to its powerful performance-enhancing capabilities. [29]

The advantages of multiple receiving antennas, such as gain and Spatial Diversity (SD), have been known and explored for a long time [30, 31, 32], while the study of transmit diversity, i.e. using two or more signals from independent sources that have been modulated with identical information-bearing signals, only started much later [33, 34]. MIMO communications were then the next step [35, 36] for antenna array technologies. Here the existence of an increased number of physical channels between the many transmits and receive antennas allows for exploitation of SD and multipath propagation, which predominantly impairs wireless channel communications, in addition to the already exploited time and frequency diversity in conventional SISO wireless systems [29].

In SISO systems, achieving higher data rates happens due to either increasing the transmission bandwidth or employing higher order constellations and increasing transmission power. Doing this can be either expensive or result in low energy efficiency, which highly degrades the capabilities of mobile devices. MIMO systems approach this problem by using the additional degrees of freedom, inherent in the higher number of antennas, to achieve higher power and SE. To do so, they make use of three types of gains: SD gain, SM gain, and array gain. SM gains are a unique characteristic of MIMO systems [29].

SD and SM gains are achieved by making use of transmitting a data segment from mul-

tiple output antennas to multiple input antennas, having their difference in the transmitted information and the result obtained from it. In SD, multiple copies of the same data are transmitted through different antennas, sharing the same physical channel to deal with multipath fading characteristics of wireless propagation, to increase the reliability of the communications. Instead, in SM the data is split into smaller segments which are transmitted simultaneously by each of the different antennas, resulting in a linear increase in information data rates. Since the SM makes use of different spatial channels, the used bandwidth remains unchanged, thus increasing the spectral efficiency. There are, nonetheless, costs to this improvement. Using a higher number of antennas implies increasing the number of data streams that must be processed, both at the transmitter and the receiver. Therefore, a higher computational complexity is required for multidimensional signal processing. While both SD and SM gains can be obtained simultaneously [23], doing so requires a compromise between the two techniques, thus decreasing a gain in favor of the other [7].

Noise immunity is also improved in MIMO systems through the array gains [37]. This is achieved due to spatial processing at the transmitter and/or receiver arrays, therefore doing coherent combining (in voltage/current) of the collected wireless signals, which in turn results in an improved SNR at the receiver, thus decreasing the noise effect in the channel [37].

With the advent of the Internet, the rapid proliferation of computational and communication devices, and services like streaming, the demand for higher data rates is ever-growing. While the wireless medium is effective at delivering high data rates at a lower cost, bandwidth and power limitations make MIMO technology indispensable in wireless communications [29].

3.2 MIMO Architectures

MIMO technology is classified into one of three categories: Point-to-Point MIMO, Multiuser MIMO, and Massive MIMO [38]. Although their functionality is based on the same concept, i.e. transmissions between multiple transmit and receive antennas, the logistics of both the Base Station (BS) and the UEs differ between each category, producing different behaviors with respective advantages and drawbacks.

3.2.1 Point-to-Point MIMO

Point-to-Point MIMO, also known as collocated MIMO, was the first form of MIMO to appear and it is the simplest one [38]. It describes a situation where a BS with a concentrated array with M antennas serves a terminal with a concentrated array with K antennas.

Disjoint time/ frequency blocks are used to serve different users via a combination of time division and frequency division multiplexing [39]. The BSs transmit a signal vector and the terminal, respectively, receives another vector at each channel use. This signal is a linear combination of transmitted signals, with the combining coefficients being determined by the propagation between the two antenna arrays. The channel, when subjected to Additive White Gaussian Noise (AWGN) at the receiver and under sufficiently high SNRs, yields, by Shannon's theory, a system spectral efficiency, expressed in bits/s/Hz, of

$$C = \log_2 \det \left(I_K + \frac{\rho_d}{M} G_d^H G_d \right) = \log_2 \det \left(I_M + \frac{\rho_d}{M} G_d G_d^H \right), \tag{3.1}$$

where G_d is the $M \times K$ frequency response matrix-valued channel and I_K is the $K \times K$ identity matrix [39] and ρ_d is the expected SNR. For this equation to be valid, it's required that the receiver knows the channel matrix, i.e. a matrix in which each value represents the channel gain, or frequency-response, between a pair of transmitting and receiving antennas. If the transmitter is also aware of it, achieving a higher performance is possible, however, it requires special efforts, and thus it is seldom done.

When in the presence of rich scattering conditions modeled by Rayleigh fading and high enough SNRs, both the UL and Downlink (DL) spectral efficiency scale linearly with $\min(M, K)$ and logarithmically with the SNR [38]. By taking this into account, it would be logical that increasing either, or both, M and K would always increase the spectral efficiency. However, this is not verifiable in practice, since point-to-point MIMO is severely limited by various factors. First off, it's hard for the propagation environment to support a significant number of data streams. This becomes a bigger problem when the terminals are composed of compact antenna arrays, in which LOS conditions become hard to deal with since the channel matrix has a minimum rank of one, therefore allowing only one data stream. Secondly, each antenna requires a dedicated independent RF chain and needs advanced signal processing to separate the data streams, thus, terminal equipment is complicated. Low SNR scenarios, which are common near the cell edge where the majority of terminals tend to be located, cause the spectral efficiency to no longer scale linearly, instead increasing slowly with the $\min(M, K)$. Lastly, while Shannon's theory delivers the result in (3.1), to approach this in

practice, requires both the receiver and the transmitter to be engaged in signal processing, which as previously mentioned is not easily done.

Another important aspect, which limits the increase in the number of antennas used, therefore making Point-to-Point MIMO non-scalable, is the need for the receiver to learn the matrix-valued channel, which requires training signals (pilots) to be used. These are mutually orthogonal when subject to peak power restrictions [40]. Thus, the training duration (in samples) needs to be higher than the number of transmit antennas. For both UL and DL together, either in TDD or FDD, the total training time τ needs to respect

$$\tau \geq M + K\,. \tag{3.2}$$

As a consequence, increasing either M or K too much will make the communication non-viable for real-time transmission. For this, Point-to-Point MIMO is restricted to $(M, K) = (8, 8)$, which is an option under current wireless standards, namely, the IEEE 802.11ac.

3.2.2 Multi-User MIMO

Multi-User MIMO (MU-MIMO) describes a scenario that results from having K single-antenna terminals being served by an M-antenna BS using the same time-frequency resources. Since each terminal no longer has a compound antenna array, terminal antenna cooperation cannot be performed and the throughput achievable for individual users is expected to be severely impacted, thus resulting in a reduction of sum-rate spectral efficiency. In reality, non-intuitively, the system sum throughput can remain unchanged through the use of proper precoding (at DL) and equalization (at UL) as long as the Channel State Information (CSI) is available. Not only that, single antenna terminals are technically simpler and LOS conditions are no longer limited to one data stream as in Point-to-Point MIMO.

MU-MIMO presents improvements to MIMO yet it is not without limitations, especially concerning scalability. To understand this, we shall present the Shannon theory expression for the system sum-throughput spectral efficiency (or sum-capacity) and its dependencies. UL-wise, the sum-capacity for MU-MIMO remains unchanged from Point-to-Point MIMO:

$$C_{\text{sum up}} = \log_2 \det\left(I_K + \frac{\rho_u}{K} G_u^H G_u\right), \tag{3.3}$$

where G_u is the channel frequency response [39]. Here only the BS is required to know the UL channel matrix and, therefore, obtain the CSI.

For the DL, the Shannon sum-capacity is given by the solution of a convex optimization problem,

$$C_{\text{sum down}} = \sup_{a} \left\{ \log_2 \det \left(I_K + \rho_d G_d D_a G^H \right) \right\}, a \geq 0, 1^T a = 1 \tag{3.4}$$

where $\mathbf{D}_a$ is a diagonal matrix whose diagonal elements comprise the M x 1 vector $\mathbf{a}$, and $\mathbf{1}$ denotes the M x 1 vector of ones [39]. This results in a higher sum-capacity compared to the Point-to-Point MIMO. However, for it to be valid and achieve near-capacity performance, it is required that both ends are aware of the channel, i.e, the BS needs to know all channels and each UE only needs to know its own DL channel. Acquiring CSI and using techniques such as dirty-paper coding/decoding (computational burden grows exponentially with M and K), is costly and quickly becomes unsustainable for real-time communications [38].

Once again, channel estimation requires using resources to transmit/receive pilot signals. For the UL channel, the BS needs to have a pilot duration (in samples) of $\tau_u \geq K$, and since the DL channel is expected to be identical as mentioned previously, no more pilots need to be sent. The UEs would also need to obtain CSI for the DL, where the pilot duration for this needs to be $\tau_d \geq M$. Therefore, the total pilot duration is restrained to $\tau_d + \tau_u \geq K + M$. However, there are other techniques [41] which allow for a lower channel estimation overhead, being dependent only on K, at the cost of the sum-capacity and vulnerable to high-mobility scenarios.

Overall, MU-MIMO brought an improvement to MIMO technology. LOS conditions don't present limitations, under the assumption that the angular separation between users is larger than the separation between the BS antennas, as well as, in general, the propagation environment becomes less detrimental to it. The terminals no longer require concatenated antenna arrays, allowing them to be simple and bringing the multiuser capability to MIMO. Nonetheless, it remains unscalable, due to the exponentially growing computation complexity in coding and decoding techniques and linear growth of channel estimation overhead with the increase of both BS antennas and UEs.

This does not imply that MU-MIMO isn't commonly used. MIMO broadcast, MIMO multiple-access-channel, and other derivations are currently used and present in wireless standards, namely from IEEE 802.11ac (Wi-Fi 5) to 802.11ax (Wi-Fi 6).

3.2.3 Massive MIMO

Massive MIMO (mMIMO) (figure 3.1) delivers a scalable version of MU-MIMO. Here, Shannon's theory sum-capacity is targeted by increasing the number of BS antennas, M,

considerably (by possibly orders of magnitude) in contrast to the previously described MIMO [39, 42].

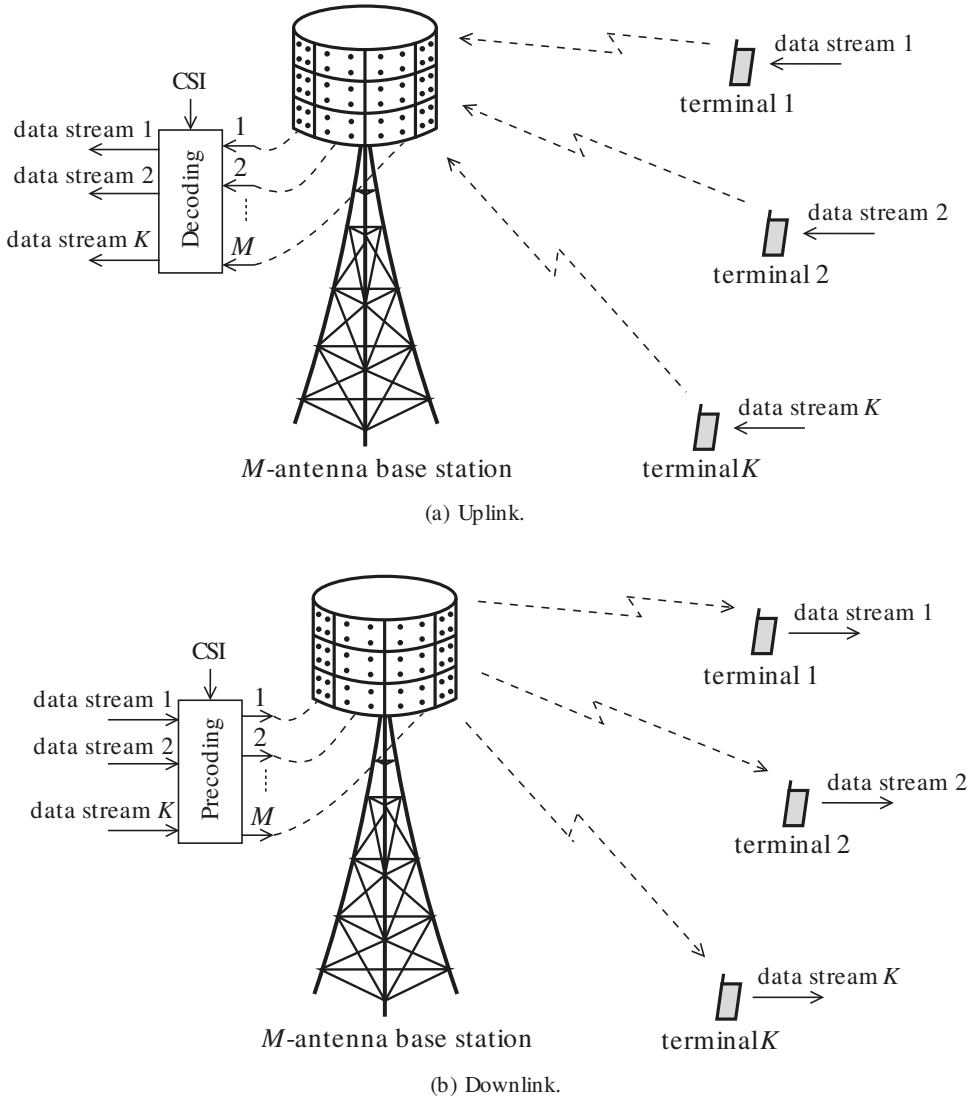

Figure 3.1: Massive MIMO (from [38]).

In conventional MU-MIMO, both the BS and the terminals needed to know the channel, which has detrimental effects on scalability. In mMIMO only the BS is required to obtain CSI. While this by itself would imply a worse performance, it is coupled with using only simple linear processing schemes (e.g., zero-forcing combining) and the channel estimation overhead being only dependent on the number of UEs. Thus, increasing the number of BS antennas has a low cost to the system. This allows M to be easily increased to values much higher than K, which lets Shannon's limit be approached nonetheless.

The increase in the number of BS antennas in mMIMO does not lead only to an increase in the system sum-capacity. Extra antennas also help by focusing energy into ever smaller

regions of space, bringing huge improvements in radiated energy efficiency. Therefore, the major improvements seen in this technology are mostly based on the possibility of increasing the BS number of antennas to a higher order.

As previously stated, mMIMO describes a scenario where a BS with M antennas serves a large number, K, of typically single-antenna UEs. Except for power and pilot control, no cooperation among BSs is done. Terminals will occupy the full-time-frequency resources concurrently through SDMA. Since only the BS knows the channel, most, if not all the processing, depends on it. While in the UL, it needs to receive the signal and recover the individual data streams, in the DL it has to ensure that each terminal receives only its intended signal. This is done once through the precoding at the BS before transmission, on possession of CSI, and by having a large number of antennas.

Similar to MU-MIMO, mMIMO holds well in both environments rich in scattering and LOS conditions, i.e. scenarios with weak multipath components. In the latter, the BS effectively creates a beam with a narrow angular window in the direction of each particular terminal. The more antennas there are in the BS, the narrower the beams which are formed are.

Obtaining CSI is done by taking advantage of TDD. The BS is not required to send any pilots, having only to measure the pilot signals transmitted by the terminals and exploit the reciprocity between the UL and DL channels. Note that while Frequency-Division Duplex (FDD) can also be used in some mMIMO systems, with training times considerably higher [43], it imposes limitations on its scalability making it seldom used.

Performance-wise, increasing the number of antennas, M, always improves the system, irrespective of the quality of the CSI. Increased sum spectral efficiencies, reduced radiated power, a higher number of served terminals and coverage uniformity are all improvements achieved by it. Paradoxically, the required signal processing and resource allocation also diminish as M increases due to a phenomenon called channel hardening. This happens as when M is large, under the law of large numbers, the channel gain, ϕ, corresponding to the channel between the terminal and the BS has its expected value, $E\{\phi\}$, which is a deterministic number. Thus, the channel is turned into a scalar channel, i.e. can be described by a single complex value, with known frequency-independent gain and addictive noise, effectively erasing the effects of small-scale fading and frequency dependence. Therefore, the use of simple schemes for resource allocation and power control, as well as, standard coding and modulation techniques, which work well since this channel typically behaves as an AWGN channel, is once more facilitated.

Through all this, Massive MIMO (mMIMO) technologies, such as the ones presented in [44, 45], are efficient ways to achieve high SE in the coverage tier of future wireless networks [24].

3.3 The Massive MIMO channel

In mMIMO technology, the effective channel associated with each terminal is a scalar point-to-point channel, though, from a mathematical perspective the system can be modeled as the transmitting signal being an $N_T \times 1$ vector, $\mathbf{x} = [\, x_1 \; x_2 \; \ldots \; x_T]$, with each vector component being a signal sent through a different antenna. On the other side, the receiver(s) will acquire an $N_R \times 1$ vector, $\mathbf{y} = [\, y_1 \; y_2 \; \ldots \; y_R]$, analogously to the transmitter, each signal is captured by an antenna. The received vector, $\mathbf{y}$, is given by

$$\mathbf{y} = \mathbf{H}\mathbf{x} + \mathbf{w} \Leftrightarrow \begin{bmatrix} y_1 \\ y_2 \\ \vdots \\ y_{N_R} \end{bmatrix} = \begin{bmatrix} h_1^1 & h_2^1 & \cdots & h_{N_T}^1 \\ h_1^2 & h_2^2 & \ldots & h_{N_T}^2 \\ \vdots & \vdots & \ddots & \vdots \\ h_1^{N_R} & h_2^{N_R} & \ldots & h_{N_T}^{N_R} \end{bmatrix} \begin{bmatrix} x_1 \\ x_2 \\ \vdots \\ x_{N_T} \end{bmatrix} + \begin{bmatrix} w_1 \\ w_2 \\ \vdots \\ w_{N_R} \end{bmatrix} \tag{3.5}$$

where $\mathbf{H}$ is an $N_T \times N_R$ channel matrix, and $\mathbf{w} = [w_1\, w_2 \cdots w_{N_R}]$ is the AWGN vector.

Each element of $\mathbf{H}$ is the channel gain obtained between each of the transmitter and receiver antennas pair, h_m^k, characterized by the large-scale fading coefficient (β_k) and the small-scale coefficient (g_m^k), such that [38]:

$$h_m^k = \sqrt{\beta_k} g_m^k, \quad k = 1, \ldots, K, \quad m = 1, \ldots, M \tag{3.6}$$

Both large-scale coefficients and small-scale coefficients need to be obtained during the channel estimation phase of communications, through the transmission of pilot signals, as succinctly explained in the previous subsection. Due to this, the base station will not have access to $\mathbf{H}$ but will know $\hat{\mathbf{H}}$, the estimated channel, instead. The detailed channel estimation will not be addressed in this thesis it is of its scope.

The received signal vector is also dependent on the chosen processing scheme. In the uplink, each antenna will receive a linear combination of the message symbols transmitted by each antenna, q_k, weighted by the square power control coefficient, η_k. Thus, $x_k = \sqrt{\eta_k} q_k$, and the m^{th} antenna receives:

$$y_m = \sum_{k=1}^{K} h_k^m \sqrt{\eta_k} q_k + w_m \tag{3.7}$$

and the received vector through all the base station becomes

$$\mathbf{y} = \mathbf{H}\mathbf{D}_{\eta}^{1/2}\mathbf{q} + \mathbf{w}, \tag{3.8}$$

where $\mathbf{D}_{\eta}^{1}/2$ is the $K \times K$ matrix with only non-zero values in the main diagonal, which are given by the square of the power control coefficients, $\sqrt{\eta_k}$ [38].

For the message symbols to be properly obtained, the base station needs to process the received vector by multiplying the received vector by a $K \times M$ decoding matrix, $\mathbf{A}$, that is a function of the channel estimate, obtaining the decoded signal $\tilde{\mathbf{y}}$.

Analogously, a similar thing happens in the DL. In this case, there are M transmitters and K receivers then, following (3.5), $\mathbf{H}_{dl}$ is an $K \times M$ matrix. Since in mMIMO no MIMO-specific processing happens at the user terminals, the base station is required to precode the transmitted vector $\mathbf{x}$, by scaling the message symbols $\mathbf{q}$ by the power control coefficient corresponding to each antenna, and then multiplying by the $M \times K$ precoding matrix, $\mathbf{A}$, such that

$$\mathbf{x} = \mathbf{A}\mathbf{D}_{\eta}^{1/2}\mathbf{q}. \tag{3.9}$$

Therefore, based on [38], collectively the terminals receive a $K \times 1$ signal,

$$\mathbf{y} = \mathbf{H}_{dl}\mathbf{x} + \mathbf{w} = \mathbf{H}_{dl}\mathbf{A}\mathbf{D}_{\eta}^{1/2}\mathbf{q} + \mathbf{w}. \tag{3.10}$$

Since $\mathbf{A}$ is dependent on the choice of the processing scheme and the estimated channel matrix, the system's performance will also be dependent on it.

For mMIMO, simple linear processing is used. The most common of these schemes are using Matched Filter (MF) and conjugate beamforming to directly oppose the frequency response of the channel [39]. Under these circumstances, $\mathbf{A}$ will be a complex conjugate transpose of the channel estimates, such that for uplink, the matrix will be

$$\mathbf{A} = \hat{\mathbf{H}}^{H}. \tag{3.11}$$

So, the decoded signal will result in

$$\tilde{\mathbf{y}} = \mathbf{A}\mathbf{y} = \hat{\mathbf{H}}^{H}\mathbf{H}\mathbf{x} + \hat{\mathbf{H}}^{H}\mathbf{w}, \tag{3.12}$$

$$\tilde{\mathbf{y}} = \begin{bmatrix} \tilde{y}_1 \\ \tilde{y}_2 \\ \vdots \\ \tilde{y}_K \end{bmatrix} = \begin{bmatrix} \mathbf{h_1^*}\mathbf{h_1}x_1 + \mathbf{h_1^*}\mathbf{h_2}x_2 + \cdots + \mathbf{h_1^*}\mathbf{h_K}x_K \\ \mathbf{h_2^*}\mathbf{h_1}x_1 + \mathbf{h_2^*}\mathbf{h_2}x_2 + \cdots + \mathbf{h_2^*}\mathbf{h_K}x_K \\ \vdots \\ \mathbf{h_K^*}\mathbf{h_1}x_1 + \mathbf{h_K^*}\mathbf{h_2}x_2 + \cdots + \mathbf{h_K^*}\mathbf{h_K}x_K \end{bmatrix} + \begin{bmatrix} h_1^* w_1 \\ h_2^* w_2 \\ \vdots \\ h_M^* w_K \end{bmatrix} \tag{3.13}$$

where $\mathbf{h}_\mathbf{k}^*$ is the k^{th} row of the $\hat{\mathbf{H}}^H$ matrix and $\mathbf{h}_\mathbf{k}$ is the k^{th} column of the $\mathbf{H}$ [38].

The MF technique has the main objective of amplifying the desired signal power, thus increasing the SNR, and works as a correlator between the estimated channel and the actual channel. In non-MIMO systems, as long as the transmitted signals are orthogonal, then it is expected that the interference terms which appear in $\hat{\mathbf{H}}^H\mathbf{H}\mathbf{x}$ are either null or negligible. Therefore only the desired signal is amplified. For MIMO, those interference terms originated from the environment propagation conditions and are, therefore, unlikely to achieve orthogonality. This implies that interference signals will also be amplified, diminishing the SINR in multi-user scenarios.

In mMIMO, a similar situation is observed as the appearance of multiple users generates cross-talk noise which can be amplified the by MF procedure. However, as long as favorable propagation conditions are achieved, increasing the number of base station antennas M results in the channel's vector from one user to another becomes asymptotically orthogonal; and the power of the desired signal to increase M times faster than the interference power [44, 46]. This, therefore, makes MF a great processing scheme for mMIMO.

Nonetheless, other types of linear precoding and decoding (or equalization techniques) can be used, for instance, Zero-Forcing (ZF) [23], in which a pseudo-inverse of the estimated channel matrix is used to channel and interference effects on the desired signal. For this, the decode matrix $\mathbf{A}$ is

$$\mathbf{A} = (\mathbf{H}^H\mathbf{H})^{-1}\mathbf{H}^H. \tag{3.14}$$

Applying this in the operation of decoding the desired signal results in

$$\begin{aligned} \tilde{\mathbf{y}} = \mathbf{A}\mathbf{y} &= (\mathbf{H}^H\mathbf{H})^{-1}(\mathbf{H}^H\mathbf{H})\mathbf{x} + \mathbf{A}\mathbf{w} \\ &= \mathbf{x} + \mathbf{A}\mathbf{w}. \end{aligned} \tag{3.15}$$

As can be confirmed by (3.15), the main objective of ZF is to separate the desired and interference signals. This makes it very effective under high SNR conditions, performing even better than MF and beamforming [39]. On the other hand, the noise component of the received signal is also amplified, which makes this processing scheme detrimental to the system's performance if the SNR is not high enough. In addition, the process of finding a pseudo-inverse matrix to the channel estimate grows with the number of the highest dimension, thus it will grow with the number of base station antennas, M. Therefore, in the context of mMIMO, ZF generally presents greater limitations than the previously shown MF processing.

3.4 Cell-free Massive MIMO

In opposition to typical cellular networks, where the service area is usually divided into small segments (cells), with each being served by an array of co-located antennas, Cell-Free (CF) mMIMO systems [8] are user-centric deployments where within the designed service area a smaller amount of UE are served simultaneously by the total (or a subset) of a much larger number of service antennas, called Access Point (AP), using the same time-frequency resources via Time-Division Duplex (TDD) [47].

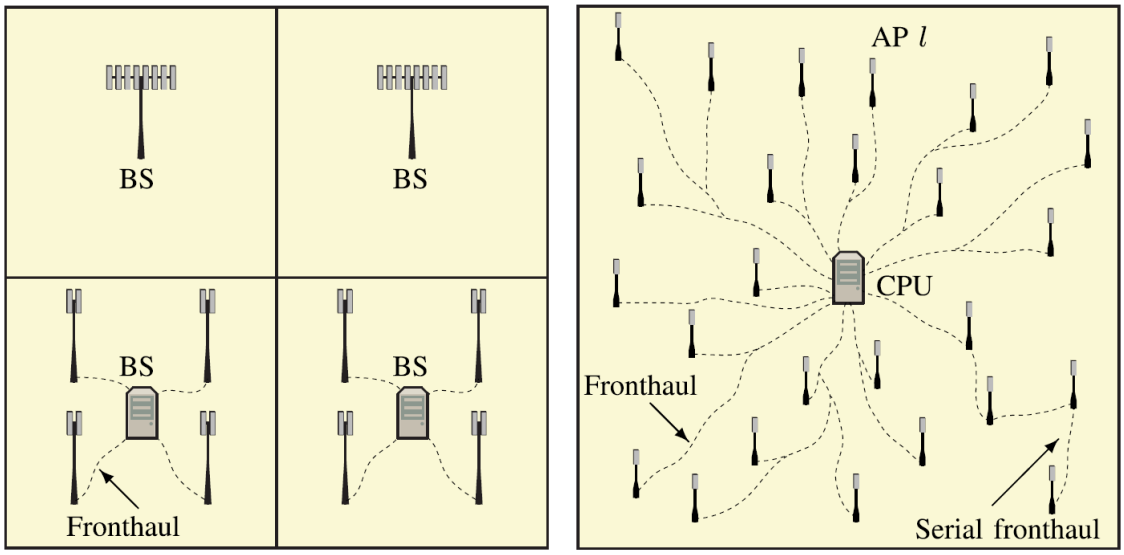

Figure 3.2: Comparison between cellular and cell-free networks network topologies (from [48]). On the left: Cellular network with mMIMO base stations having co-located arrays (top) or distributed arrays (bottom). On the right: CF mMIMO network.

These CF systems (see figure 3.2) are composed of at least one Central Processing Unit (CPU) which is responsible for system coordination, the various APs spread throughout the system, and a front-haul connection used to exchange information between the previous components. Different CPUs are interconnected by a backhaul connection which also connects to the core network. The information exchanged between the APs and the CPU is usually limited to payload data only, with instantaneous CSI being acquired and used only locally at each AP.

CF mMIMO brings a lot of benefits when compared to traditional cellular mMIMO networks due to strong macro-diversity and multi-user interference suppression capabilities [49]. Under sophisticated AP selection schemes [50, 51], an optimized number of APs can be selected to serve each UE, leading to an increase in Energy Efficiency (EE) by more than ten times over a centralized mMIMO scheme [52] and more than two times over cellular mMIMO

networks by relying on max-min power control [53]. Due to this high EE and low amount of antenna elements in each AP, CF mMIMO offers a flexible and cost-efficient deployment compared to the large base station employed in network MIMO, and since the APs are more distributed through the service area, the distance between them and each UE is, in general, substantially reduced, which results in a more uniform coverage and quality of service, as demonstrated by [47], where CF mMIMO showed significantly better average DL throughput than small-cells systems. Lastly, while the channel hardening seen in a centralized mMIMO scheme might not be valid in these deployments, since distributed APs' antennas might impose some spatial correlation between the signals arriving from different specific AP at a UE, [54] shows that it can be observed for very low path loss exponents. Table 3.1 shows an overview of CF mMIMO performance over centralized cellular mMIMO network.

Table 3.1: Comparison between centralized massive MIMO, network MIMO, and CF massive MIMO (from [49]).

Architecture	**Centralized**	**Network**	**CF**
Number of Antennas	large	moderate	large
Deployment Cost	high	high	low
Macro Diversity	small	moderate	large
Channel Hardening	strong	weak	moderate
Favorable Propagation	strong	weak	moderate
Uniform Coverage	bad	moderate	good
Energy Efficiency	large	small	very large
Channel Estimation	global	global	local
Front-haul Resources	small	large	moderate

Under CF mMIMO, uplink data detention can be performed in three different ways: fully distributed, being done at each AP; centralized, all payload data is grouped and decoded in the CPU; or partially distributed. The SE of this deployment under four different levels on uplink data detention is studied in [48] and shows that assuming Minimum Mean-Square Error (MMSE) is used, the centralized approach has the highest SE at the cost of higher front-haul requirements.

mmWave communications have a straightforward connection to CF mMIMO, as both techniques are very suitable for indoor short-range communications. In the latter, to mitigate path loss, the distance between APs and UEs is significantly reduced. This also helps by

providing macro diversity gains for reducing the detrimental shadowing effects, thus making it suitable to operate at the mmWave bands. Nonetheless, some impairments still stand in the way of systems that combine these two technologies, for example, the channel impulse response of such systems being too sparse in both time and angular domains [55].

While CF mMIMO presents a lot of benefits over other traditional networks, they still hold some issues that need to be solved in practical deployment. The limited capacity of back/front-haul connections, which can become an even greater problem for centralized data detention architecture, and network synchronization needed to serve UEs with coherent joint transmission from multiple APs [56], are some of the most prominent issues.

Close antenna processing, reducing front-haul capacity requirements, and linear AP placement to the extent that synchronization is only required between a small group of APs and its neighbor, are known solutions to the predicaments above. These can be found on Radio Stripe technology [56], making it one of the most promising CF mMIMO deployments.

4 Radio Stripes Architecture

As highlighted in Chapter 2, mmWave communications bring key advantages for the next generation of wireless systems, such as much larger frequency bands and smaller antenna elements, allowing the deployment of large antenna aggregates. While the use of mmWave increases FSPL attenuation, thus decreasing inter-user and inter-cell interference, the large aggregates can enable energy focusing (beamforming) to serve a particular user at a greater distance with a higher power.

These benefits can leverage the deployment of mMIMO technology, discussed in Chapter 3, relying on a large amount of BS antennas to use only simple linear processing and exploit the channel hardening effect.

Cell-Free systems can be achieved with mMIMO technology and can lead to an increase in EE and a higher, more uniform average SE throughout the coverage area. The Radio Stripe, developed by Ericsson, is seen as one of the technologies that will enable the use of these topologies.

Thus, this chapter will focus on presenting this practical deployment, by exploring its practical advantages and developing the channel model which will be used to study its behavior in this thesis.

4.1 Radio Stripes

RSs [12] are characterized as a 1-D improved antenna arrangement with close antenna processing for distributed Massive MIMO. They are considered a flexible and cost-effective architecture for CF mMIMO topologies and can be used in a multitude of cases, in both outdoor and indoor areas. Some examples are densely populated city squares, stadiums, train stations, factories, and others.

In the RS system, APs are constituted by antenna elements aggregated to circuit-mounted chips with a digital signal processor called Antenna Processing Units (APUs). These include

power amplifiers, phase shifters, filters, modulators, and A/D and D/A converters. The APs are serially located inside a protective case of cable or a stripe and are connected to a shared bus which works as a front-haul connection to one or more CPUs, and synchronization and power supply, as seen in figure 4.1. This makes the required front-haul connection more cost-efficient [56].

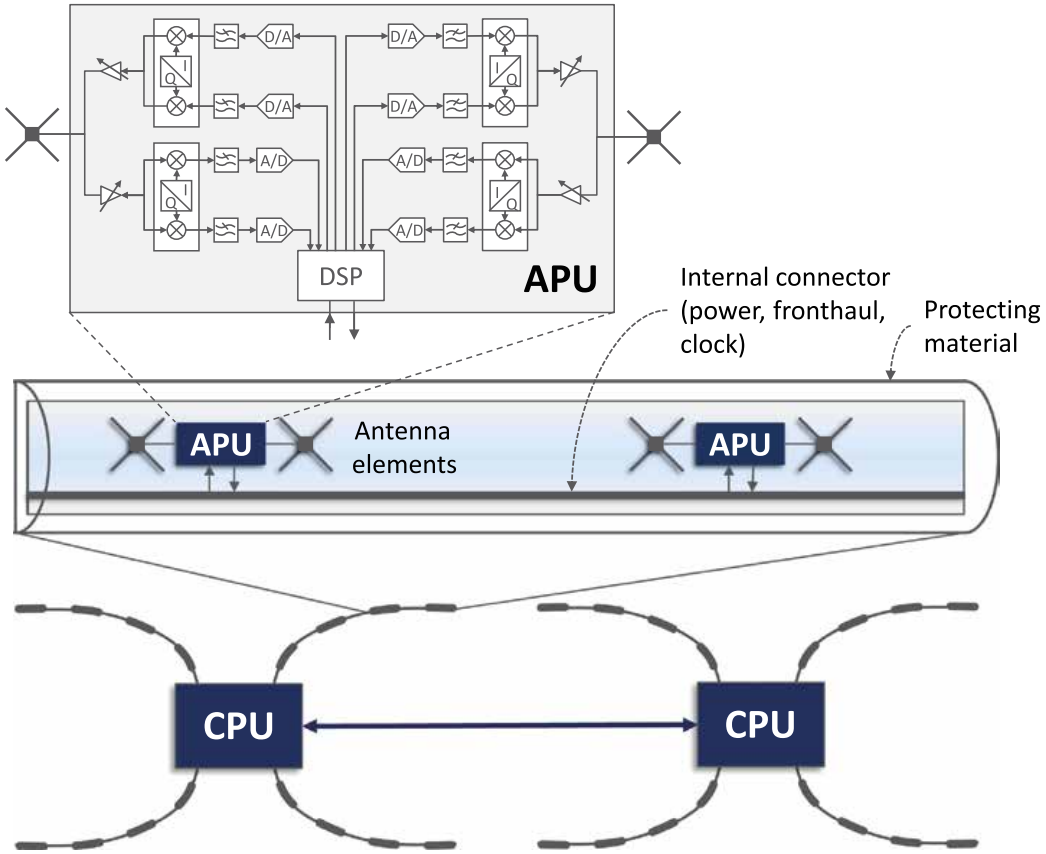

Figure 4.1: Radio stripe system design (from [56]).

Depending on the frequency range for which the system is designed, RS could have either distributed antennas, assuming sub-6 GHz frequencies, or multiple co-located antenna elements for mmWave bands. Since the number of these elements is assumed to be large, the transmit power at each element can be significantly reduced. This in turn results in low heat dissipation and a higher EE. Small volume and weight, low cost, and easy installation are other characteristics expected from RSs.

The serial architecture allows for the generation of a cumulative signal in the UL, where each APU sequentially receives a transmitted signal, multiplies it with the previously calculated combining vectors and adds its result to that of the previous APU, and then forwards to the next one until it reaches the CPU. This helps to severely reduce front-haul capacity requirements, a major practical issue in CF mMIMO deployments. Reducing the strain in

front-haul capacity is also possible by diminishing the number of APs which serve each user and selecting the best subset of them [47, 52, 57], especially considering that if the serviced area and number of APs are great enough, only a handful of them will belong to the subset which provides 95% of the received power [56].

4.2 Radio Stripe Transmission Channel

We will now define a channel model for wireless RS CF mMIMO communications. This channel will be used in Chapter 5 to study the average user capacity at both sub-6 GHz and mmWave frequencies.

Channel Model Considerations

The main objective of this model is to understand the limits of RS Uplink channel capacity under perfect LOS conditions. To do such, the wireless channel will be modeled through a narrow-band deterministic model, dependent mostly on array geometry and UEs (ideal isotropic radiators) location relative to the APs elements.

On array geometry, most considerations will fall under its total size and antenna element spacing. The RS will be considered a linear array of size L embedded with M equal planar antenna elements, having a uniform spacing between each other. The antenna spacing, Δ_s, is assumed great enough to allow uniform gain with no correlation between received signals at different elements, i.e. no mutual coupling between antenna elements will be considered. Therefore, the received signal can be seen as a sum of the signals received at each element of the array, which highly simplifies the signal processing as well as the study of these channels.

All dimensions metrics are normalized by the previously defined antenna element spacing, Δ_s, to obtain an FSPL-independent antenna spacing and easier analysis results. With this, the number of antenna elements, M, will then be directly equivalent to the array size. This normalization does not put at stake the previous assumption of no mutual coupling between antenna elements.

Notice that in scenarios with a limited size, and independently of it, edge effects will be ignored for sake of simplicity, assuming they are never strong enough to be considered relevant to any channel capacity calculation.

The focus on LOS communication is justified by the distributed nature of CF mMIMO networks and the expectable development of RS technology for operating at mmWave. In such scenarios, due to a great number of antennas spread along the serviced area, it is

expected that most users will always be close and in LOS condition to the APs with the highest contribution to channel performance. In addition, at mmWave, due to the high FSPL and lower reflection at obstacles, the number of received rays under multipath propagation is trivial and their power is negligible compared to the main LOS ray, assuming it exists. Thus, we can focus on this component of the transmission since it most likely will be the dominant one in any received signal.

Working with a large array causes most UE to be excepted to be located in its near-field of the array, which is achieved at the Fraunhofer distance [16], but on the far-field of its antenna elements, as explained in Chapter 2. This implies that, for analysis purposes, it is convenient to model the linear antenna array as a contiguous surface, greatly simplifying the mathematical treatment. This is especially relevant in cases with a high density of antennas as in systems operating at mmWave frequency bands. Nevertheless, it is important to notice that, due to this the result can be more accurately interpreted as a limit to what can be achieved instead of an exact value of the system performance. The results of this treatment [58] have been shown to be a great approximation, and the same will be proved further on.

In this way, the RS will be modeled as a line composed of antennas close enough to be considered a continuum. Regarding APUs, these are assumed to be paired with the antennas in such a way that it is possible to provide partially distributed processing, without introducing delays, regardless of the size of the RS.

Lastly, noise-wise, a simplified deterministic channel model with Additive White Gaussian Noise (AWGN) was assumed. The transmitted signals are independent Gaussian variables with zero-mean and unit variance, such that the channel capacity is presented in bits per channel use is

$$C = \log_2(1 + \text{SINR}). \tag{4.1}$$

with SINR being the Signal-to-Interference-plus-Noise Ratio.

Therefore, in the following subsections, we will derive two models, both for LOS scenarios, respectively for single-user and multiuser scenarios, and their respective average channel capacities.

4.2.1 Received Signal in Single-User Scenario

For simplicity of the model, we will start by ignoring the third dimension, assuming propagation happens only in the xy-plane. We assume an UE positioned at coordinates (X,Y) of a given space and in LOS of an infinite size RS linear antenna array at the xz-plane (see

figure 4.2), operating at a frequency f_c with respective wavelength, λ. The UE transmits the data symbols $u[m]$ with power P_t and duration T. If the transmit time for the signal to the antenna array is negligible compared to T, then, based on [58], the received baseband signal from this UE, s, at the location $(x, y = 0)$ and at instant t, is

$$s(x,t) = \sum_{m=-\infty}^{\infty} h_{X,Y}(x)\sqrt{P_t}u[m]\,\mathrm{sinc}_T(t - mT) + n(x,t) \tag{4.2}$$

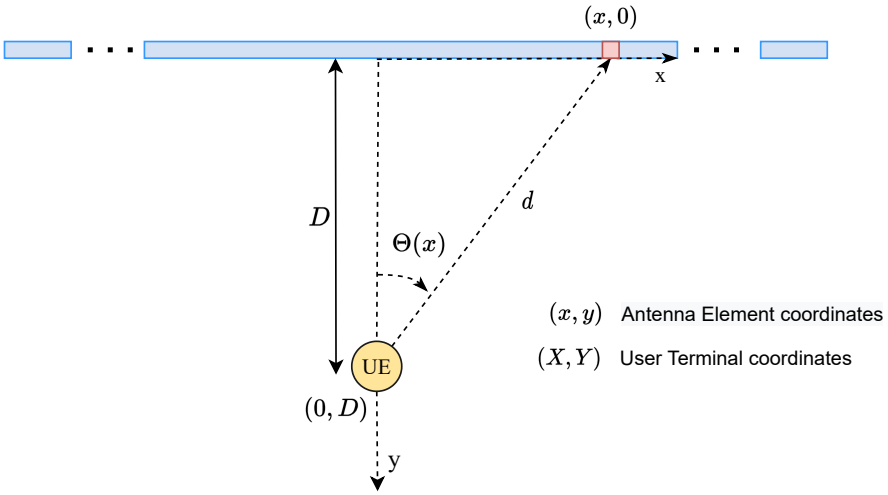

Figure 4.2: Radiating model of transmitting signal to the infinite size RS for UE deployed in LOS of the linear antenna array, at a distance, D, from its closest point. RS is positioned in xz-plane and the UE is assumed to be centered with the array.

with $h_{X,Y}(x)$ being the channel impulse response, '$\mathrm{sinc}_T(t)$' being a unit-energy sinc pulse with two-sided bandwidth $W = 1/T$, and *n(x,t)* being the noise term, which is independent over the various locations of the antenna array and modeled as wide-sense stationary (WSS) Gaussian process with zero-mean and a spatial PSD N_0 at each position.

The scalar-valued complex channel $h_{X,Y}(x)$ is modeled with FSPL attenuation, given by (2.5), and a phase shift, such that:

$$h_{X,Y}(x) = \sqrt{G(\theta(x))}\frac{\lambda}{4\pi d}\exp(-jkd) \tag{4.3}$$

with an isotropic transmitter, i.e. $G_t = 1$, and the following parameters:

- d is the euclidean distance between the UE, which is always centered due to the assumed infinite length of the RS, and the location $(x, 0)$ of the antenna array, given by

$$d = \sqrt{x^2 + D^2}\ . \tag{4.4}$$

- k is the wave number given as $k = 2\pi/\lambda$.
- $\theta(x)$ is the Angle of Arrival (AoA) from the user signal in the array antenna at the x position and its cosine is given by $\cos(\theta) = D/d$.
- $G(\theta(x))$ is the gain pattern of the antenna array element. Since the considered antennas have planar elements (Fig. 4.3), the gain pattern is given by

$$G(\theta(x)) = \frac{4\pi A_e(\theta(x))}{\lambda^2} = \frac{4\pi A \cos(\theta(x))}{\lambda^2} \tag{4.5}$$

  where A_e is the effective antenna element area and A is the antenna element area [59], hereafter assumed to be normalized (for sake of simplicity and without loss of generalization), i.e. $A = \Delta x \times \Delta z = 1$, as depicted in figure 4.3.

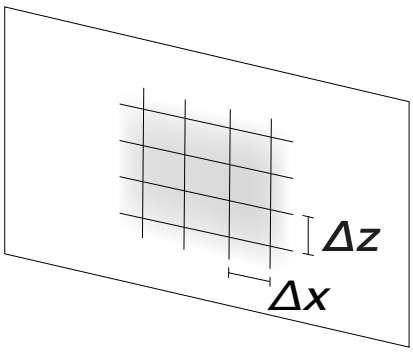

Figure 4.3: Illustration of two-dimensional LIS made from closely spaced planar antenna elements. Each element has an area of A = ΔxΔz = 1. The center-to-center spacing along the z-axis and x-axis is Δz and Δx respectively (adapted from [59]).

The resulting channel for transmission between an UE and a specific point of the RS is then described as

$$h_{X,Y}(x) = \frac{1}{2}\sqrt{\frac{D}{\pi d^3}}\exp\left(-j\frac{2\pi d}{\lambda}\right) . \tag{4.6}$$

After applying optimum processing with a temporal correlator to each transmitted signal, i.e. Matched Filter (MF), the resulting received signal at sampling time mT is

$$\begin{aligned} \hat{s}[m] &= \sqrt{P_t}\int_{x\in C} h^*_{X,Y}(x)\left(s(x,t) \star \mathrm{sinc}_T(t)\big|_{t=mT}\right)\, dx \\ &= P_t u[m]\int_{x\in C} h_{X,Y}(x)h^*_{X,Y}(x)\, dx + w[m] \\ &= P_t \phi u[m] + w[m] \end{aligned} \tag{4.7}$$

where the line C is the domain of integration with a bijective parametrization given by the respective ends of the RS, $w[m]$ is the effective discrete noise after the match filtering procedure and ϕ is the gain coefficient obtained after coherent combining, i.e. the array gain, and is described as

$$\phi = \int_{x \in C} h_{X,Y}(x) h^*_{X,Y}(x)\, dx\,. \tag{4.8}$$

The received signal power is then defined by $P_s = P_t \phi$.

For the signal received through an infinite linear antenna array, as presented in the referred figure 4.2, the coefficient ϕ becomes (see Appendix A)

$$\begin{aligned} \phi &= \int_{x \in C} \left(\frac{1}{2} \sqrt{\frac{D}{\pi d^3}} \right)^2 \exp\left(-j \frac{2\pi d}{\lambda} \right) \exp\left(j \frac{2\pi d}{\lambda} \right) dx = \\ &= \int_{-\infty}^{\infty} \frac{D}{4\pi d^3}\, dx = \int_{-\infty}^{\infty} \frac{D}{4\pi \left(D^2 + x^2\right)^{3/2}}\, dx = \frac{1}{2\pi D}\,. \end{aligned} \tag{4.9}$$

Thus, in a single-user scenario, the channel capacity in bits per channel use is given by

$$\begin{aligned} C &= \log_2 \left(1 + \frac{P_t \phi}{N_0} \right) \\ &= \log_2 \left(1 + P_t \frac{1}{2\pi D N_0} \right). \end{aligned} \tag{4.10}$$

Formulations for Finite Length Arrays

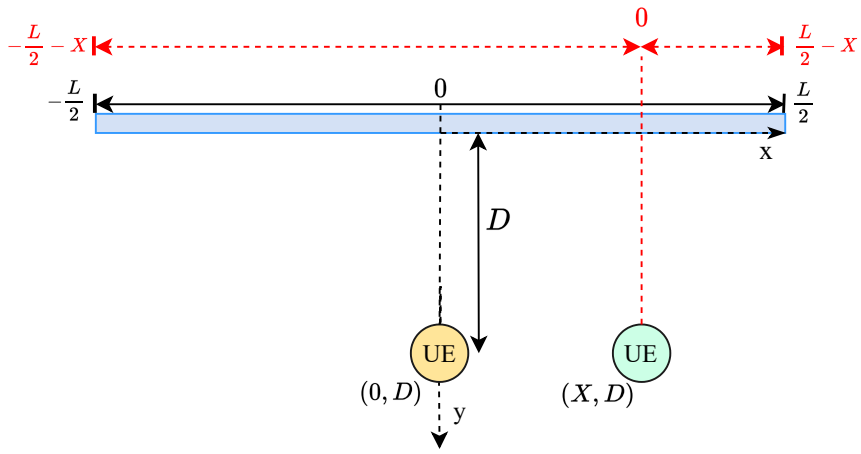

Figure 4.4: Radiating model of transmitting signal to the finite size RS of length L for UEs deployed in line-of-sight of the antenna array, at a distance, D, centered (yellow) and non-centered (green).

Initially, we defined that the RS extends infinitely, allowing our study to be focused on

UEs distance to the closest point in the array. Changing this scenario by limiting the stripe, and adding its size as a new variable, increases the complexity of the model in various ways.

If the size of the array is limited, then so will be the array gain and the received signal power ends up being reduced. Secondly, a finite length stripe implies the existence of antenna border elements and, in a real-world scenario, the appearance of edge effects, i.e., the antenna elements in the further extremes of our stripe will behave slightly differently than the remaining ones. As previously stated, these effects will be ignored.

The integral in (4.8) is now bound by the stripe length, L. Therefore, the received signal power coefficient, ϕ, for a single user being served by a RS with length L and positioned centered with it is (see Appendix A)

$$\begin{aligned}\phi &= \int_{x\in C}\left(\frac{1}{2}\sqrt{\frac{D}{\pi d^3}}\right)^2 dx = \int_{-\frac{L}{2}}^{\frac{L}{2}}\left(\frac{1}{2}\sqrt{\frac{D}{\pi d^3}}\right)^2 dx \\ &= \int_{-L/2}^{L/2}\left(\frac{D}{4\pi\left(D^2+x^2\right)^{3/2}}\right) dx = \frac{1}{2\pi D}\frac{L}{\left(4D^2+L^2\right)^{1/2}}\,.\end{aligned} \tag{4.11}$$

For a non-centered user, $X \neq 0$, the integral in (4.11) does not present a closed form. However, we can see this situation as a user centered with a non-symmetrical stripe, resulting in the following integral (see Appendix A)

$$\begin{aligned}\phi &= \int_{x\in C}\left(\frac{1}{2}\sqrt{\frac{D}{\pi d^3}}\right)^2 dx = \int_{-\frac{L}{2}-X}^{\frac{L}{2}-X}\left(\frac{1}{2}\sqrt{\frac{D}{\pi d^3}}\right)^2 dx = \\ &= \frac{1}{4\pi D}\left(\frac{\frac{L}{2}-X}{\sqrt{D^2+(\frac{L}{2}-X)^2}} - \frac{-\frac{L}{2}-X}{\sqrt{D^2+(-\frac{L}{2}-X)^2}}\right)\,.\end{aligned} \tag{4.12}$$

Notice that since the dimensions are normalized to the antenna spacing, L effectively corresponds to the number of antenna elements composing the RS.

4.2.2 Received Signal in Multiuser Scenario

As mentioned in Chapter 2, multiuser transmissions are expected to happen over the time-frequency resources, resulting in interference signals and crosstalk noise appearing. These can become highly degrading to the system's performance, substantially limiting the reliability and throughput, if they are not properly dealt with.

Equalization techniques, such as the MF and ZF shown in Chapter 3, decode the received signal by making use of the channel estimation, limiting interference, becomes essential in

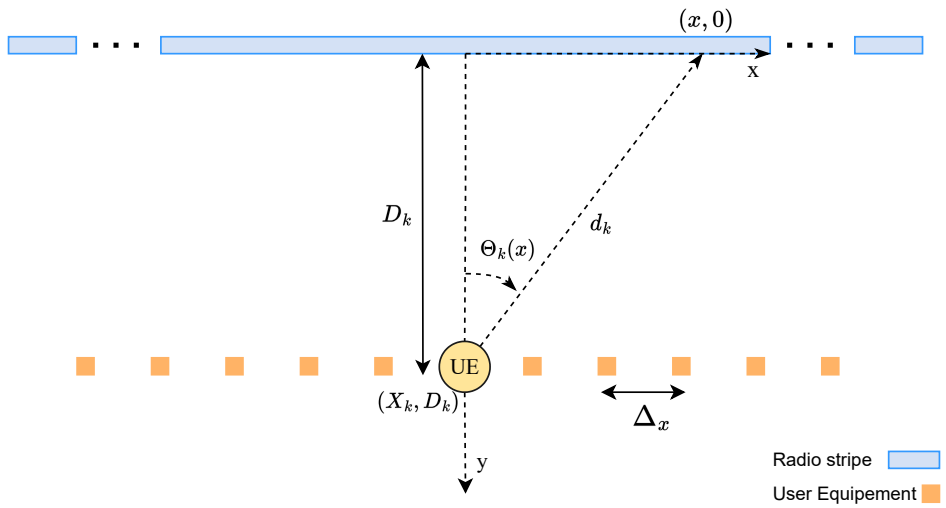

Figure 4.5: Radiating model of transmitting signal to the infinite size RS for UEs deployed in line-of-sight of the antenna array, at a distance, D, from its closest point and a spread between themselves by a distance Δx.

this scenario. While ZF was shown to be better in dealing with high interference scenarios, since the number of antenna elements in the defined RS topology tends to be high, the MF procedure remains a preferable choice, due to its much lower complexity.

Mathematical Formulations over Infinite Length Arrays

Let us assume a scenario with K users with (X_k,Y_k) be the position of the k^{th} user and d_k the distance from this to the RS AP at position $(x, 0)$ (as shown in figure 4.5), such that

$$d_k = \sqrt{(x - X_k)^2 + D_k^2}\ . \tag{4.13}$$

Based on the signal model defined for the single-user scenario, the received narrow-band signal at the location $(x, 0)$ of the antenna array is now described as the sum of all received K users' transmitted signals, such as

$$s(x,t) = \sum_{k=0}^{K} \sum_{m=-\infty}^{\infty} h_{X_k,Y_k}(x)\sqrt{P_k}u_k[m]\,\mathrm{sinc}_T(t - mT) + n(x,t), \tag{4.14}$$

applying the MF process results that the received signal at sampling time mT equals

$$\begin{aligned}\hat{s}_k[m] &= \sqrt{P_k}\int_{x\in C} h^*_{X_k,Y_k}(x)\left(s(x,t)\star \mathrm{sinc}_T(t)\big|_{t=mT}\right)\,dx \\ &= \sum_{l=0}^{K-1}\sqrt{P_tP_l}u_l[m]\int_{x\in C} h_{X_k,Y_k}(x)h^*_{X_l,Y_l}(x)\,dx + w_k[m] \\ &= \sum_{l=0}^{K-1}\sqrt{P_tP_l}\phi_{k,l}u_l[m] + w_k[m],\end{aligned} \tag{4.15}$$

where $\phi_{k,l}$ is defined as

$$\phi_{k,l} = \int_{x\in C} h_{X_k,Y_k}(x)h^*_{X_l,Y_l}(x)\,dx. \tag{4.16}$$

Thus, based on (4.6), the coefficients $\phi_{k,l}$ are given by

$$\begin{aligned}\phi_{k,l} &= \int_{x\in C} h_{X_l,Y_l}(x)h^*_{X_k,Y_k}(x)\,dx \\ &= \int_{x\in C}\frac{1}{2}\sqrt{\frac{D_l}{\pi d_l^3}}\exp\left(-j\frac{2\pi d_l}{\lambda}\right)\times\frac{1}{2}\sqrt{\frac{D_k}{\pi d_k^3}}\exp\left(j\frac{2\pi d_k}{\lambda}\right)\,dx \\ &= \left(\frac{\sqrt{D_l}\sqrt{D_k}}{4\pi}\right)\int_{x\in C}\frac{1}{(d_kd_l)^{3/2}}\exp\left(-j\frac{2\pi(d_l-d_k)}{\lambda}\right)\,dx\end{aligned} \tag{4.17}$$

with d_k and d_l being dependent on x as seen in (4.13).

Lastly, the average channel capacity for each UE becomes

$$C = \left(\frac{1}{K}\right) log_2\left(det\left(\mathbf{I}_K + \frac{\mathbf{G}}{N0}\right)\right). \tag{4.18}$$

where K is the number of UEs and $\mathbf{G}$ is the corresponding hermitian matrix resulting from the MF process on the received signal, $\mathbf{G} = \hat{\mathbf{H}}^H\mathbf{H}$, as shown in (3.12) and (3.13). The (k,l) element of $\mathbf{G}$, $g_{k,l}$, is given by

$$g_{k,l} = \sqrt{P_kP_l}\phi_{k,l} \tag{4.19}$$

and signifies the effect that the l^{th} UE signal has in the k^{th} signal throughout all of the RS.

Since no closed-form expressions can be achieved by solving the integral in (4.17), no different formulation will be presented for the limited-size RS channel performance. The performance results for the multiuser case will need to be computationally calculated, at which point the RS's length can be easily restricted to study the limited RS behavior.

5 Performance Results

In this chapter, the results of the RS channel performance study, using the model defined in Chapter 4, are presented. The performance, and the average UE channel capacity, were evaluated as a function of UE distance and position to the RS center, as well as the influence of the RS length for the single-user case. For the multiuser scenario, the main focus was to observe how UE quantity, density, and distance to RS effect the system performance on different RS length categories.

The simulation's fixed fixed parameters are presented in table 5.1, while any variable will be mentioned together with the given results. All dimensions are normalized by the antenna spacing Δ_s. UE transmission power was chosen to be unitary for simplification, avoiding the introduction of power coefficient schemes. Operating frequencies were varied between 3 GHz for sub-6 GHz bands and 30 GHz for mmWave bands for multiuser scenarios only, due to the FSPL propagation being independent of the operating frequency, as shown by (4.6). Finally, notice that since T_sW, i.e. the coherence interval, is assumed to be unitary, channel capacity will be expressed in bits/s/Hz, therefore characterizing the Spectral Efficiency (SE).

Table 5.1: Simulation parameters.

Parameter [Unit]	**Value**
Noise Figure [dB]	9
Noise Temperature [K]	290
Noise Variance [dBm]	-96
Transmission Power [mW]	1
Transmit Antenna Gain	1
TW	1

The proposed model, which assumes the RS as a continuum of antennas and is, thus, based on integral calculations, will be compared to a more realistic discrete deployment of RS (linear 1D antenna aggregate spaced by Δ_s, typically to be $\lambda/2$), in order to test

for the validity and to understand the RS performance. The discrete deployment channel capacities will also be given by (4.18) but the power coefficients, $\phi_{k,l}$, (considering discrete signal processing at the RS), specified by the following sum:

$$\begin{aligned}\phi_{k,l} &= \sum_{n\in E} h_{X_l,Y_l}(x) h^*_{X_k,Y_k}(x) \\ &= \left(\frac{\sqrt{D_l}\sqrt{D_k}}{4\pi}\right) \sum_{n\in E} \frac{1}{(d_k d_l)^{3/2}} \exp\left(-j\frac{2\pi(d_l - d_k)}{\lambda}\right)\end{aligned} \tag{5.1}$$

where E is the antenna set and d_k is the distance between the k^{th} UE and the n^{th} AP, located at $(x[n], 0)$, such that

$$d_k = \sqrt{(x[n] - X_k)^2 + D_k^2}\,. \tag{5.2}$$

Notice that, for $k = l$, (5.1) derives the discrete array gain coefficient utilized in the single-user capacity.

5.1 Single-User Case

As previously stated, the single-user scenario case focus on how a single UE position and the RS length influence its channel capacity. To do so, the channel capacity was first analyzed for an infinite length case, using (4.10), for a UE centered with the RS and at a distance (D) of its plane. These results (figure 5.1a) are compared with a discrete computation of capacity, based on the array gain from (5.1) with $k = l$.

While small differences are visible at close distances to the array, both calculations hold extremely similar results. This observation is reinforced by the absolute difference in figure 5.1b, where the value is only relevant as D closes to 0. Notice, however, that this divergence holds no importance in a real-world case. The reason for this is two-fold. First, the FSPL equation does not describe extremely short propagation paths, as can be proven by assuming an UE positioned infinitely close to the RS, which results in the possible scenario of an infinite channel capacity, which is a naturally impossible result. Second, for LOS conditions to be expected to happen regularly, RS has to be placed so that the signal can't be easily blocked, therefore making these scenarios very unlikely to happen, e.g. near the ceiling.

The effects of RS length, L, in channel capacity can be studied based on the power coefficient, ϕ, in (4.11). Figure 5.2a shows three scenarios, for different values of distance, D, for which the RS-centered UE channel capacity varies in function of the RS length, L. As more antenna elements are added, the received signal power improves, and the SE grows

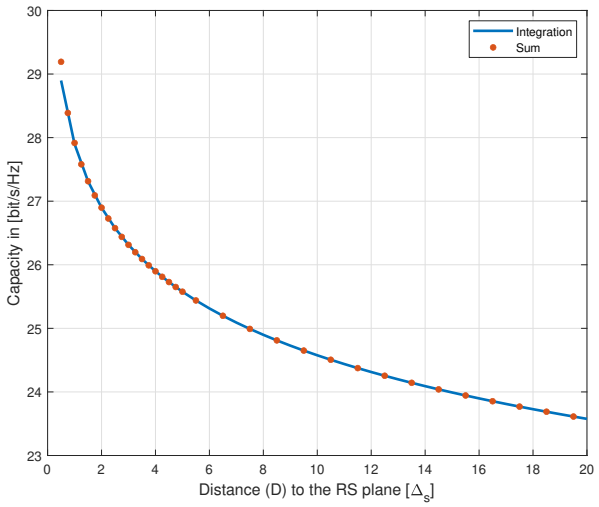

(a) Overlapped results from both calculations.

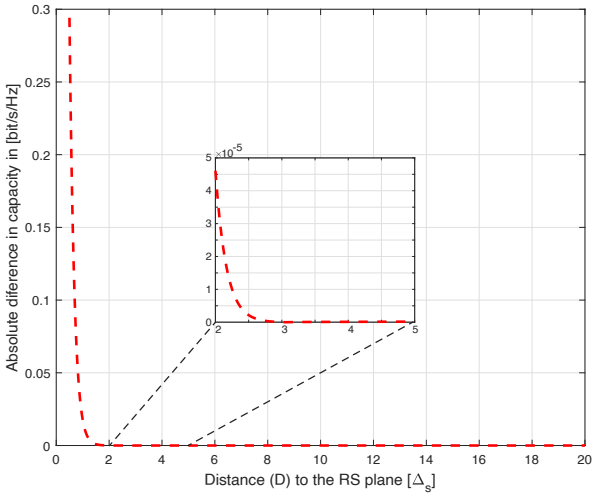

(b) Absolute difference between results.

Figure 5.1: Comparison between (4.10) and a discrete computation of capacity for a single UE center with an infinite RS at a distance D for communications operating at 3 GHz.

logarithmically. However, since the array will only grow outwards, the path loss suffered while propagating to these new elements also increases. Thus, while increasing the array size always shows benefits capacity-wise, the improvement per additional AP decreases with the length of the RS.

Expected user distance also plays a role in this, as seen in the previously mentioned figure. As the D increases, the limits of channel capacity, imposed by the infinity RS scenario and calculated in (4.10), become harder to achieve. The main reason for this, is the relation between the distance to the RS plane and the distance to each individual element, or infinitesimal segment, d, tending to 1 as the UE gets further away. Then, the received signal power at any particular element becomes less relevant in comparison to the remaining ones. Thus, requiring the length to be greater the further from the RS plane the UE is positioned, in order to achieve the same percentile of maximum channel capacity.

While this behavior is similar for both integral and summation computations, the latter approaches the established limit much faster. This may indicate that, for studies with very small lengths, i.e. number of APs, the expressions of the closed form presented in chapter 4, may deliver improper results. However, under reasonable antenna spacing, e.g. of $\Delta_s = \lambda/2$, the requirements for the actual length of the RS array are fairly low.

Lastly, UE position, besides its distance D, also influences system performance due to the AoA. Capacity is not uniform with the distance to the antenna elements (as can be observed in figure 5.2b), degrading faster as the UE gets further to the sides of RS, i.e. away

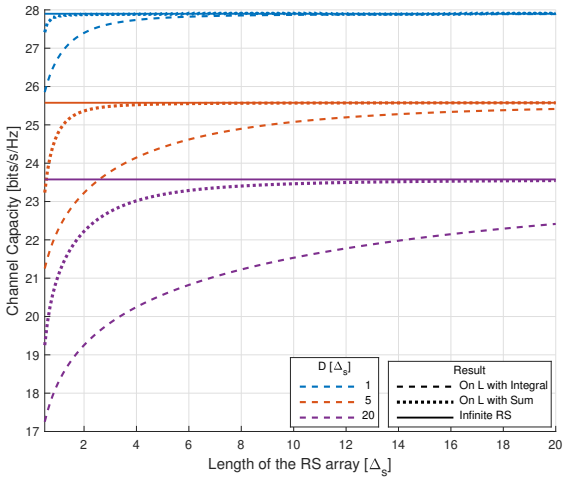

(a) UE channel capacity as a function of RS length at varied distances D.

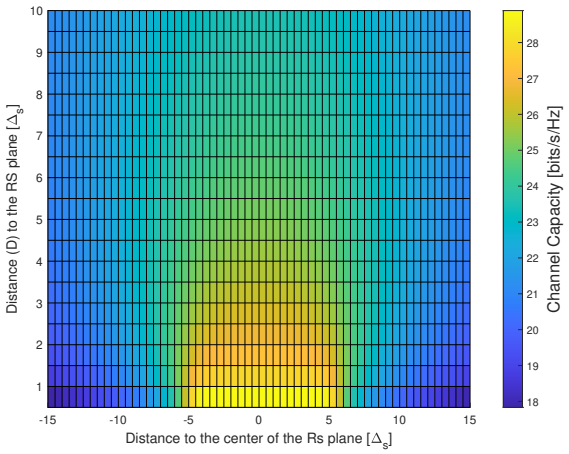

(b) UE channel capacity in function position with a RS of length 10 Δ_s.

Figure 5.2: Results UE channel capacity as a function of the RS array size and UE position, operating at 3 GHz.

from its center at $(0, 0)$. The cause for this is the directional nature of the RS antenna array. The antenna elements' gain pattern in (4.5), depends on the angle $\theta(x)$, i.e. the signal AoA. When an UE behaves as described above, the angle will tend to $\pi/2$, shrinking the antenna effective area and highly decreasing the antenna gain.

5.2 Multiuser Case

Multiuser scenarios introduce interference, which should be mainly dependent on the following factors: transmission frequency, number of UE (K), and user spacing (Δx). The study made for this case is based on the illustration in figure 4.5 and shows how average UE channel capacity varies with each of the mentioned variables, in different categories of RS length. The scenarios tested are divided into three based on these categories:

- Large Radio Stripe: Length is defined to be substantially greater than the area covered by UE.
- Small Radio Stripe: Length is either smaller or approximately the same length as the area covered by UE.
- Effective Radio Stripe Length: The perceived array length for each UE is variable and determined by the distance to the array, D, and SE restriction.

Table 5.2 lists all the used values for the referred variables in each scenario, however, not all combinations will be displayed for the sake of concision.

Table 5.2: Simulated values for the multiuser case.

Variable	**Values**		
	Large RS	**Small RS**	**Effective RS Length**
Length (L) [Δ_s]	[500, 1000, 2000]	[50, 100, 150]	500 (Max.)
User Spacing (Δx) [Δ_s]	[0.1, 0.5, 1, 5, 10]	[0.5, 1, 5, 10]	[0.1, 0.5, 1, 5, 10]
Number of Users (K)	[5, 10, 20, 30]	[20, 30]	[5, 10, 20, 30]
Frequency (f_c) [GHz]	[3, 30]		

5.2.1 Large Radio Stripe

In this scenario, a RS with a length reasonably larger than the space covered by adjacent UEs serves all users in the same time-frequency domain with all APs available. The effect of UE density, based on their spacing and quantity was evaluated under the same conditions, i.e. same array length and frequency, and can be observed in the graphs displayed in figure 5.3. Here, the first important divergence between the integral and summation computational results appears. As the interference is introduced, the discrete computations of the developed a model presents a worse, yet more realistic, average SE.

The difference seen between the two results has its origin in the way the signal phases are dealt with during the MF process, i.e. in (4.17). When an integral is used, as long as the antenna array has enough APs which desired signal reception for each UE, the computation is capable of canceling out the interference phase between signals, resulting in better performance. Thus, as long as L is big enough, the integral computation is not affected by interference.

As D increases, the difference between the two computations slowly becomes negligible due to the received signal phase from two different UE becoming, at the APs which hold the strongest influence. Then, the path loss component becomes dominant in the power coefficient ($\phi_{k,l}$) calculation.

As the number of UE (K) increases, the interference component grows in power, and the SINR drop, originating worse average SE. The same happens inversely with UE spacing, albeit with different degrees of intensity. Nevertheless, the interference effect is only notice-

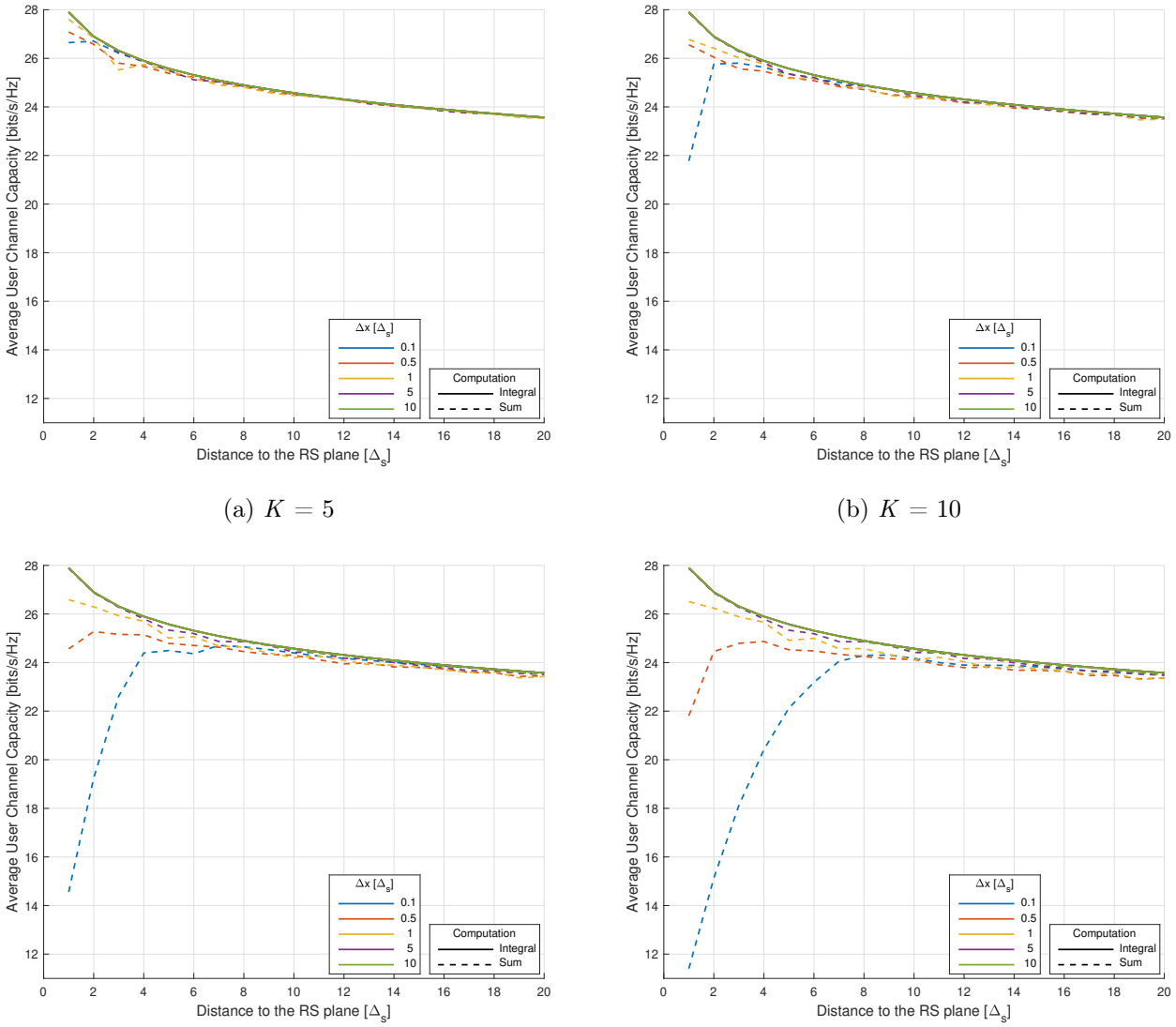

(a) $K = 5$ (b) $K = 10$

(c) $K = 20$ (d) $K = 30$

Figure 5.3: Average channel capacity for K UE, with Δx spacing between each other, as a function of the distance to a RS with $L = 500$ and operating at a frequency of 3 GHz.

able when both variables present "matching values", i.e. a high number of users placed very close to each other. For $K = 5$ (figure 5.3a), even at the closest spacing of $\Delta_s = 0.1$, the interference effect could be considered negligible, having a similar performance as 30 UE with maximum spacing (figure 5.3d).

Figure 5.4 characterizes the study of RS length and frequency effect on the interference scenario. A comparison of the results from different frequency bands shows that operating at higher frequency bands presents a visible benefit to the multiuser case. While the path loss defined in the channel model does not differ based on operating frequency, the phase shift between the signals is affected, diminishing the interference signal, as observed in figures 5.4b and 5.4d. Thus, increasing f_c lends itself to diminishing interference which allows for higher

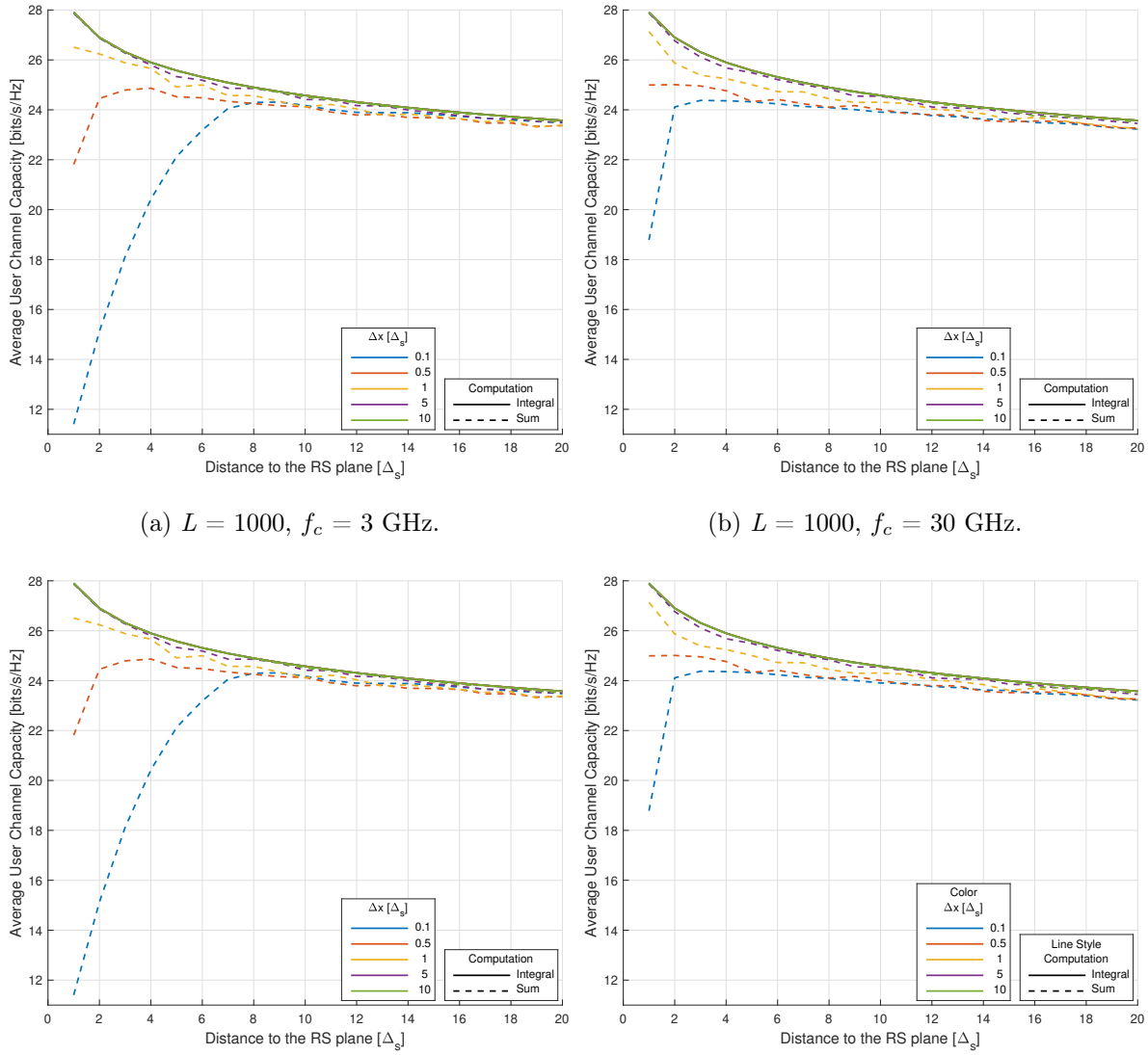

(a) $L = 1000$, $f_c = 3$ GHz.

(b) $L = 1000$, $f_c = 30$ GHz.

(c) $L = 2000$, $f_c = 3$ GHz.

(d) $L = 2000$, $f_c = 30$ GHz.

Figure 5.4: Average channel capacity for $K = 30$ UE, with Δx spacing between each other, as a function of the distance to a RS variable size and operating at a frequency of 3 GHz.

SE to be achieved in regions close to the RS, where the interference effect is the strongest.

Lastly, figure 5.4 presents a simulation with two distinct RS sizes, respectively two and four times the one used for figure 5.3. In both cases, the resulting average channel capacities hold no significant differences between themselves and the previous results for $L = 500$. Therefore, increasing the array length unrestrictedly, i.e. in comparison to the expected space occupied by UE, is shown to have no improvements to the system's performance, while considering only signal propagation.

5.2.2 Small Radio Stripe

In real-world cases both the RS and the UEs are expected to be limited in space under the same conditions, resulting in the array length being either smaller or approximately the same size as the UE coverage length. Therefore, figure 5.5 presents performance results for systems using RS with small lengths.

In the previous section, it was shown that RS becoming too large showed no practical SE improvement. The simulation with a smaller array in figure 5.5d, where $L = 150$, shows that decreasing it to undersized array results in the average SE dropping significantly.

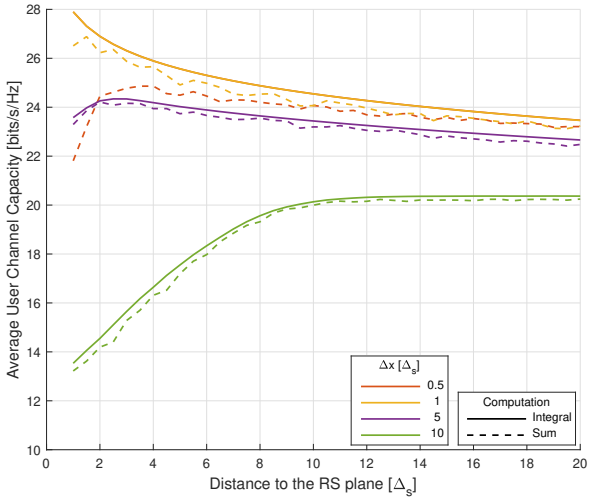

(a) L = 100, f_c = 3 GHz.

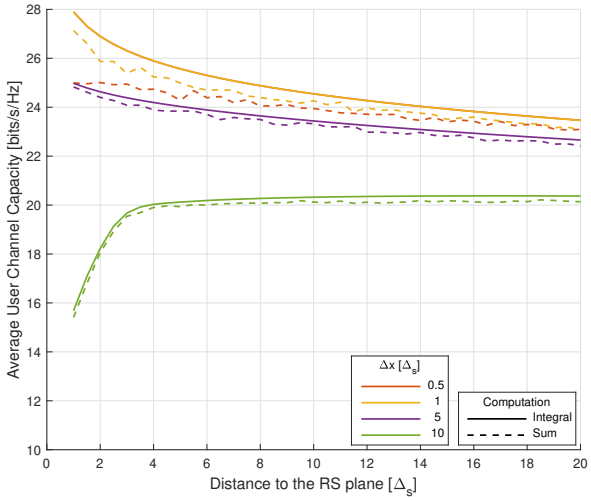

(b) L = 100, f_c = 30 GHz.

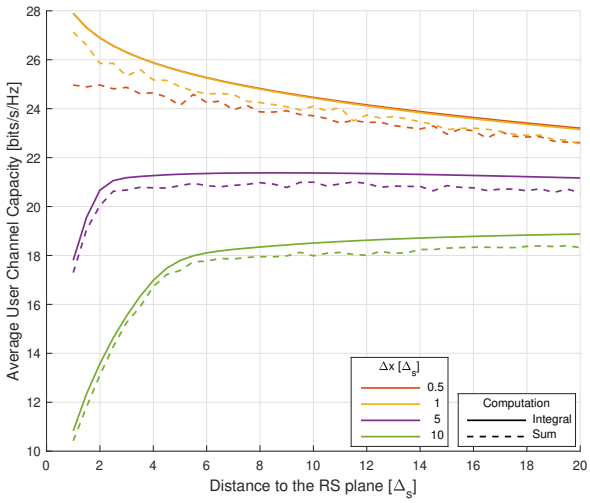

(c) L = 50, f_c = 30 GHz.

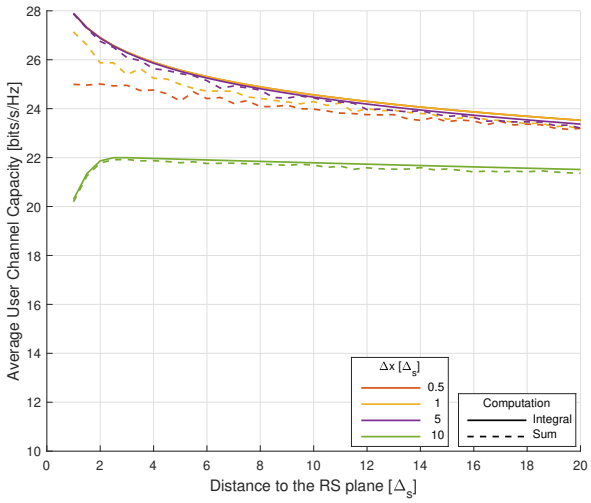

(d) L = 150, f_c = 30 GHz.

Figure 5.5: Average channel capacity for K=30 UE, with Δx spacing, as a function of the distance for 'Small array' RS with varied length (L) and operating frequencies (f_c).

The previously stated performance drop happens specifically in the case with maximum spacing between UE. Here, the overall length occupied by the UEs, given by $K\Delta x$, reaches

and overextends the size of the array. This leads to border UEs channel capacity getting worse as there are fewer APs close to them, resulting in an overall average lower performance.

The degradation is most noticeable when the difference between UE spread and array size is large, being visible for $\Delta x = 10$ in all presented cases in figure 5.5, and increased with it. However, even when the sizes between the antenna array and the user spread to match, e.g. figure 5.5d for $\Delta x = 5$, performance loss already grows faster with D, in comparison to larger arrays.

The initial lack of performance for lower D and high Δ_x is the result of two factors. Firstly, the antenna directivity, as seen in the single-user case (figure 5.2b). As border UEs are positioned close to the RS plane but further away to the side of it, the AoA becomes unfavorable, leading the desired received signal power to be low. As D grows, this angle becomes suitable and its effect gets corrected.

The second cause is the interference effect, which significantly impacts the system at lower D. As RS is not big enough to serve all users, the desired signals from border UE are highly affected by it. Thus, interference affects both methods, making them consistent between themselves under these conditions.

As operating frequency was shown to have an impact on interference signals, increasing it, operating in mmWave frequency bands, leads to an improvement in SE at lower values of D. However, the effect caused by the AoA remains unchanged, continuing to be observable when Δ_x is large.

5.2.3 Effective Radio Stripe Length

The last case presents a RS with an effective length, $\hat{L}$, restricted to the necessary to achieve the desired percentile of the maximum SE for a given D, based on (4.10). This means that the desired signal from a given UE is only evaluated at the nearest $\hat{L}(D)$ length of the RS, as shown in figure 5.6.

Channel capacity was shown to grow logarithmically based on the stripe length, and the requiring L to achieve a given percentile of its maximum increases exponentially with D (figure 5.2a). To deal with this, $\hat{L}$ is restricted to a maximum length, in table 5.2, when a minimum that guarantees the defined condition inferior to this value does not exist.

Limiting the RS to based on 95% SE (figure 5.7) provides an overall slight improvement to the system performance. For integral computation, due to the way signals phase are dealt with during the MF process, all cases deliver better capacity than in previous scenarios,

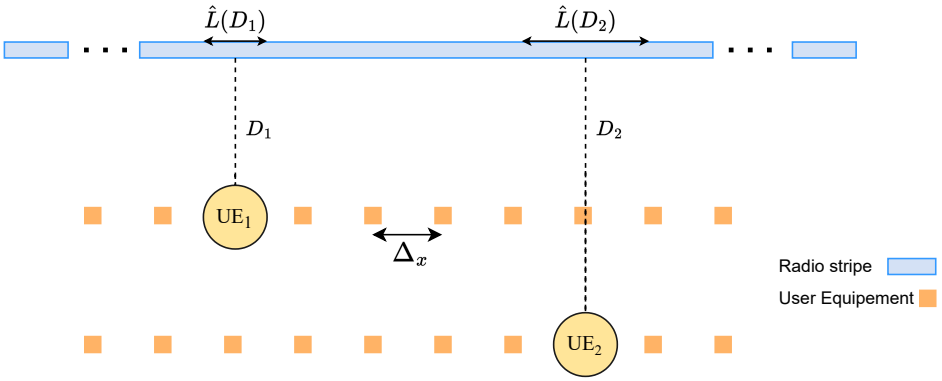

Figure 5.6: Example of the effective RS length ($\hat{L}$) for UEs deployed in LOS of the antenna array, at different distance D.

especially for the highest user spacing, since it will no longer consider the signal power at distant APs where the influence from remote UEs' signals is stronger.

Close to the RS, the resulting $\hat{L}$ is very small and the number of APs considered is severely reduced. As computation with summation can not deal with signal phases in the same way as the integral, it becomes very susceptible to interference, which in cases with a high density of UE, causes small RS length to critically worsen the system performance. However, as D grows, $\hat{L}$ increases, resulting in more APs to be considered, which is especially beneficial to border UEs, Thus, system performance grows and both computations match, delivering slightly better average channel capacity than for simple large arrays.

The overall behavior of the computational results remains the same as for large array cases, as no UE gets either low coverage or an unfavorable AoA at the closest APs. While increasing the number of UE leads to higher interference and lower performance, operating at higher frequencies, results in reduced interference effects for summation computations, although it continues to be highly affected by it.

Finally, decreasing the desired target percentile of SE, in this case, to 90% (figure 5.8), results in a worse performance. The negative effects previously mentioned for the computational results with summation only get worsen. As the condition gets lessened, $\hat{L}$ gets lower and the interference effect dominates until farther distances. The improvement provided due to the discarded signal power from interfering UE at far away APs does not compensate for the decrease in SE imposed by the restriction condition.

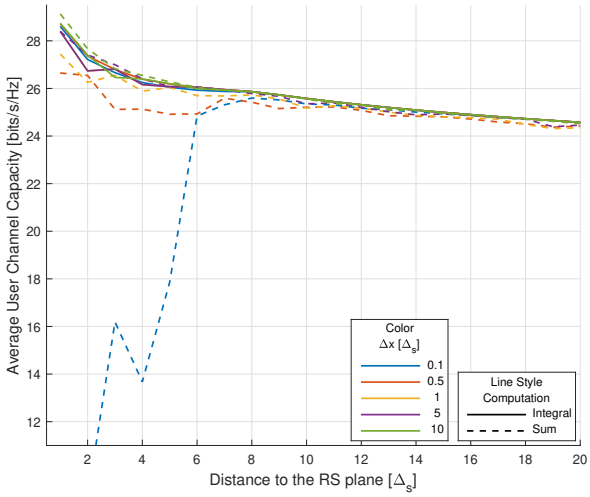

(a) $K = 10$, $f_c = 3$ GHz.

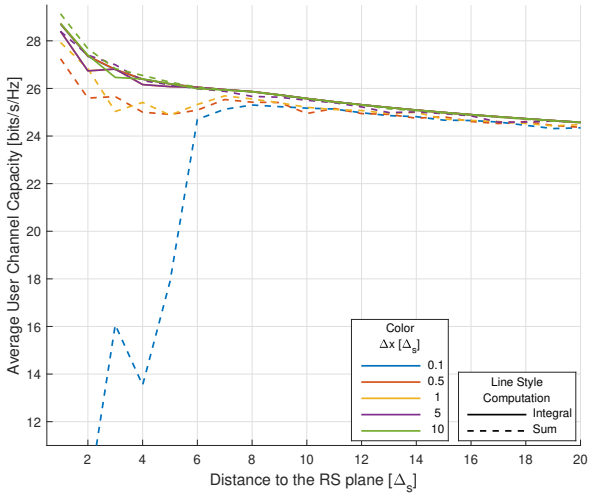

(b) $K = 10$, $f_c = 30$ GHz.

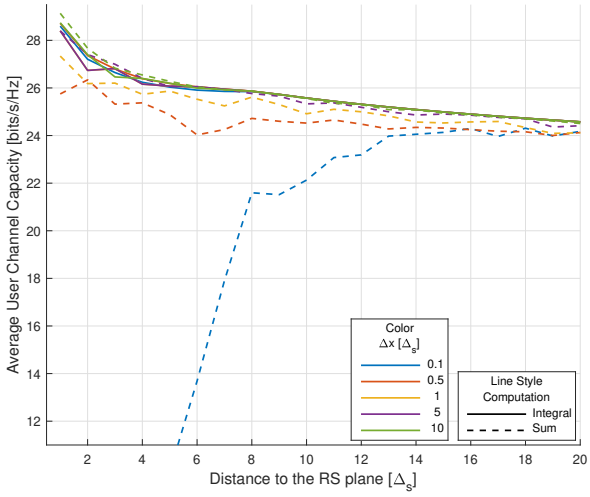

(c) $K = 30$, $f_c = 3$ GHz.

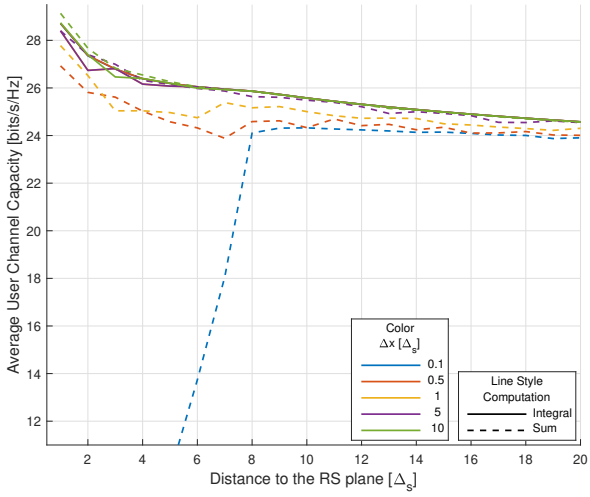

(d) $K = 30$, $f_c = 30$ GHz.

Figure 5.7: Average channel capacity for K UE, with Δx spacing between each other, as a function of the distance to a RS with a variable perceived length ($\hat{L}$), restricted to the condition of achieving 95% SE and operating at a frequency of f_c GHz.

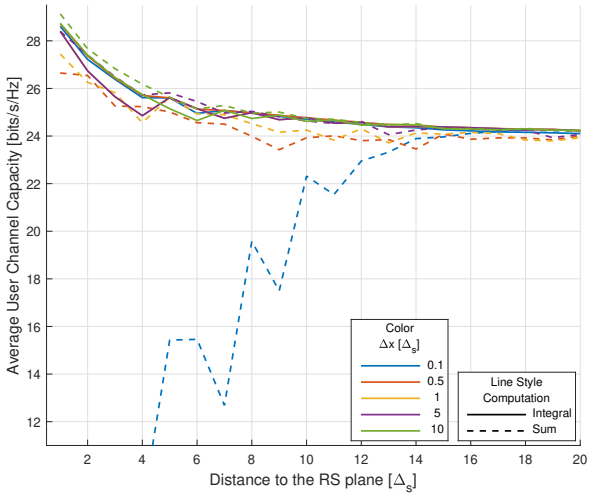

(a) $K = 10$, $f_c = 3$ GHz.

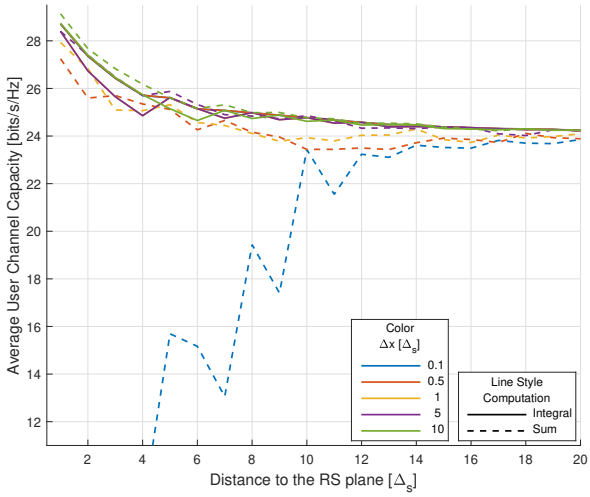

(b) $K = 10$, $f_c = 30$ GHz.

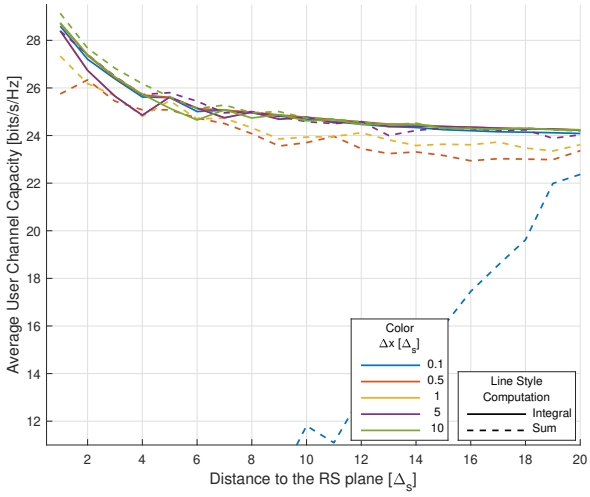

(c) $K = 30$, $f_c = 3$ GHz.

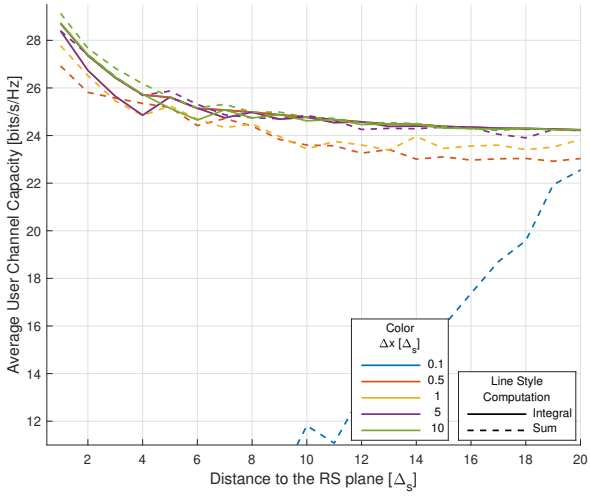

(d) $K = 30$, $f_c = 30$ GHz.

Figure 5.8: Average channel capacity for K UE, with Δx spacing between each other, as a function of the distance to a RS with a variable perceived length, $\hat{L}$, restricted to the condition of achieving 90% SE and operating at a frequency of f_c GHz.

5.3 Observations

The model defined in chapter 4 characterizes the UL transmission for both single and multiuser LOS communications using an assumption of continuous surfaces. For the first case, it was shown extremely consistent with a discrete approach, except in a scenario with a very limited RS size, i.e. number of antennas, while for multiuser cases, the RS model was shown to have some discrepancies concerning high interference in close range. However, as the distance to the array increase, both models reach consistency. Both exceptions are easy restrictions to overcome in real-world scenarios, assuming a reasonable antenna spacing.

Regarding the RS behavior, high directivity originated by unfavorable AoA outside of the was shown to be highly detrimental to small RS, as border UE is not properly served by it. Large RS shows no direct improvement in growing excessively irrespectively to the UE spread. However, doing so might provide improvements due to other advantages, such as channel hardening or enabling RS segmentation with different effective lengths, which was shown to be able to improve performance. For real-world usage, an optimization algorithm for RS dynamical segmentation and AP allocation is expected to be used under these conditions, improving performance even further and possibly lowering front and backhaul capacity requirements.

Lastly, different operation bands were shown to have strong implications on the system's performance. Systems operating at mmWave frequencies were able to deal with interference at a close range of the RS better than ones at sub-6 GHz. However, it is important to notice that since all distances were normalized to antenna spacing, assuming that this varies with wavelength would imply that the scenario would be considered to either shrink or expand as a function of it. Nevertheless, the behavior would remain the same, albeit with a higher path loss at higher frequencies. This can be dealt with by increasing the number of antennas as explained in Chapter 2, resulting in an array with the same actual size but with a higher form factor.

6 Conclusions

This work focused on the study of Radio Stripes, a promising distributed Cell-Free mMIMO technology for beyond 5G communication networks, capable of achieving higher uniform SE coverage with high reliability in a designated area.

A deterministic transmission model for Uplink communication under LOS conditions was developed, describing the RS as a continuous one-dimensional LIS with a MF procedure applied to the received narrow-band signal. Closed-form expressions for array gain, at both infinite and limited stripe length, were achieved.

The provided model was used to understand the transmission channel behavior in function of transmission wavelength, UEs density, position, and distance to the APs, for different sized RS in both multiple and single-user cases.

In the single-user scenario, the array gain, and respectably the channel capacity, was shown to be inversely proportional to the UE distance to the RS and grow logarithmically with the antenna array length. Position-wise, the channel was shown to be highly vulnerable to unfavorable AoA, with its performance degrading faster as the UE gets further to the sides in comparison to their distance to the RS plane.

Interference was the main object of study in the multi-user scenario. The assumption of contiguity on RS antenna elements causes the channel computations to be impervious to interference under RSs which guarantees that each UE is served by a high amount of APs. This condition can not hold for border terminals on RSs with lengths approximate or smaller than the UEs spread, as it causes low SE at closer distances to the array, where interference is the strongest and AoA is more detrimental. Using a simple effective RS length restriction was shown to improve system performance, by ignoring the detrimental effects of interference in APs with bad desired signal reception, owning to being positioned away from transmitter UE.

Application of mmWave frequency bands in RS was shown to provide a system more resilient to inter-user interference effects, improving the average SE at closer distances, when

compared to systems operating at sub-6 GHz bands. While some higher path loss results from transmitting at higher frequencies, this could be compensated by the higher array form factor inherent to it. Even higher performance could be achieved due to the large bandwidth available in these bands.

In conclusion, Radio Stripe deployments were shown able to serve the network users adequately under realistic criteria for any reasonable antenna spacing, in both mmWave and sub-6 GHz bands. Furthermore, we described that some RS lengths and UEs' placements are prejudicial for SE. Nonetheless, the resulting system's performance degradation is expected to be lessen under the usage of power optimization schemes, giving rise to a more uniform coverage than what was observable. Lastly, proper segmentation of RS was proven directly more beneficial to performance than simply increasing the availability of APs.

6.1 Future Work

This thesis presented a transmission model for RS and analyzed the characteristics of their practical deployments based on deterministic LOS behavior. The obtained results were satisfactory and provided some do's and don'ts for the deployment of this state-of-the-art CF mMIMO implementation. Nonetheless, no power or AP allocation schemes were considered, perfect CSI was assumed and, due to the high AP count, only the MF procedure was included in the studies. Thus, some suggestions for future work direction are the implementation of the mentioned schemes with optimization metrics based on SINR and SE. In cases with a more limited number of APs, extending it further by implementing ZF and MMSE receivers with and without perfect CSI, also presents an interesting future work. Lastly, the design of a probabilistic simulator with CSI acquisition through pilot signals and embodied with the previous optimization schemes should be referred to as a target objective, as it will present various challenges.

7 Bibliography

[1] Wendy Arianne Günther, Mohammad H Rezazade Mehrizi, Marleen Huysman, and Frans Feldberg. Debating big data: A literature review on realizing value from big data. *The Journal of Strategic Information Systems*, 26(3):191–209, 2017.

[2] Jeffrey G Andrews, Stefano Buzzi, Wan Choi, Stephen V Hanly, Angel Lozano, Anthony CK Soong, and Jianzhong Charlie Zhang. What will 5g be? *IEEE Journal on selected areas in communications*, 32(6):1065–1082, 2014.

[3] Anutusha Dogra, Rakesh Kumar Jha, and Shubha Jain. A survey on beyond 5g network with the advent of 6g: Architecture and emerging technologies. *IEEE Access*, 9:67512–67547, 2020.

[4] Jian Wang, Aixiang Jin, Dai Shi, Lei Wang, Hui Shen, Dan Wu, Liang Hu, Liang Gu, Lei Lu, Yan Chen, et al. Spectral efficiency improvement with 5g technologies: Results from field tests. *IEEE journal on selected areas in communications*, 35(8):1867–1875, 2017.

[5] Suhas N Diggavi, Naofal Al-Dhahir, Anastasios Stamoulis, and A Robert Calderbank. Great expectations: The value of spatial diversity in wireless networks. *Proceedings of the IEEE*, 92(2):219–270, 2004.

[6] Angel Lozano and Nihar Jindal. Transmit diversity vs. spatial multiplexing in modern mimo systems. *IEEE Transactions on wireless communications*, 9(1):186–197, 2010.

[7] Ui-Kun Kwon, Gi-Hong Im, and Jong-Bu Lim. Mimo spatial multiplexing technique with transmit diversity. *IEEE Signal Processing Letters*, 16(7):620–623, 2009.

[8] Elina Nayebi, Alexei Ashikhmin, Thomas L Marzetta, and Hong Yang. Cell-free massive mimo systems. In *2015 49th Asilomar Conference on Signals, Systems and Computers*, pages 695–699. IEEE, 2015.

[9] Tianwei Hou, Yuanwei Liu, Zhengyu Song, Xin Sun, and Yue Chen. Mimo-noma networks relying on reconfigurable intelligent surface: A signal cancellation based design. *IEEE Transactions on Communications*, PP:1–1, 08 2020.

[10] Qingqing Wu and Rui Zhang. Towards smart and reconfigurable environment: Intelligent reflecting surface aided wireless network. *IEEE Communications Magazine*, 58(1):106–112, 2020.

[11] Yuanwei Liu, Xiao Liu, Xidong Mu, Tianwei Hou, Jiaqi Xu, Marco Di Renzo, and Naofal Al-Dhahir. Reconfigurable intelligent surfaces: Principles and opportunities. *IEEE Communications Surveys & Tutorials*, 23(3):1546–1577, 2021.

[12] Pål FRENGER, Jan HEDEREN, Martin HESSLER, and Giovanni INTERDONATO. Improved antenna arrangement for distributed massive mimo, Jun 2018.

[13] Zabih Ghassemlooy, Luis Nero Alves, Stanislav Zvanovec, and Mohammad-Ali Khalighi. *Visible light communications: theory and applications*. CRC press, 2017.

[14] Cory Beard and William Stallings. *Wireless communication networks and systems*. Pearson, 2015.

[15] Ieee standard definitions of terms for antennas. *IEEE Std 145-1983*, pages 1–31, 1983.

[16] Constantine A Balanis. *Antenna theory: analysis and design*. John wiley & sons, 2015.

[17] Sathish Chandran. *Adaptive antenna arrays: trends and applications*. Springer Science & Business Media, 2013.

[18] Xuefeng Yin and Xiang Cheng. *Propagation channel characterization, parameter estimation, and modeling for wireless communications*. John Wiley & Sons, 2016.

[19] Harald T Friis. A note on a simple transmission formula. *Proceedings of the IRE*, 34(5):254–256, 1946.

[20] Theodore S Rappaport et al. *Wireless communications: principles and practice*, volume 2. prentice hall PTR New Jersey, 1996.

[21] Tzi-Dar Chiueh and Pei-Yun Tsai. *OFDM baseband receiver design for wireless communications*. John Wiley & Sons, 2008.

[22] David M Pozar. *Microwave engineering*. John wiley & sons, 2011.

[23] Andrea Goldsmith. *Wireless communications*. Cambridge university press, 2005.

[24] Emil Björnson, Jakob Hoydis, and Luca Sanguinetti. Massive mimo networks: Spectral, energy, and hardware efficiency. *Foundations and Trends in Signal Processing*, 11(3-4):154–655, 2017.

[25] Theodore S Rappaport, Shu Sun, Rimma Mayzus, Hang Zhao, Yaniv Azar, Kevin Wang, George N Wong, Jocelyn K Schulz, Mathew Samimi, and Felix Gutierrez. Millimeter wave mobile communications for 5g cellular: It will work! *IEEE access*, 1:335–349, 2013.

[26] Robert W Heath, Nuria Gonzalez-Prelcic, Sundeep Rangan, Wonil Roh, and Akbar M Sayeed. An overview of signal processing techniques for millimeter wave mimo systems. *IEEE journal of selected topics in signal processing*, 10(3):436–453, 2016.

[27] Ming Xiao, Shahid Mumtaz, Yongming Huang, Linglong Dai, Yonghui Li, Michail Matthaiou, George K Karagiannidis, Emil Björnson, Kai Yang, I Chih-Lin, et al. Millimeter wave communications for future mobile networks. *IEEE Journal on Selected Areas in Communications*, 35(9):1909–1935, 2017.

[28] David Tse and Pramod Viswanath. *Fundamentals of wireless communication*. Cambridge university press, 2005.

[29] Ezio Biglieri, Robert Calderbank, Anthony Constantinides, Andrea Goldsmith, Arogyaswami Paulraj, and H Vincent Poor. *MIMO wireless communications*. Cambridge university press, 2007.

[30] William C. Jakes. *Microwave Mobile Communications*. IEEE, 1994.

[31] Robert A Monzingo and Thomas W Miller. *Introduction to adaptive arrays*. Scitech publishing, 2004.

[32] Keith W Forsythe, Daniel W Bliss, and Catherine M Keller. *Multichannel adaptive beamforming and interference mitigation in multiuser CDMA systems*, volume 1. 1999.

[33] Armin Wittneben. Basestation modulation diversity for digital simulcast. In *[1991 Proceedings] 41st IEEE Vehicular Technology Conference*, pages 848–853. IEEE, 1991.

[34] Vijitha Weerackody. Diversity for the direct-sequence spread spectrum system using multiple transmit antennas. In *Proceedings of ICC'93-IEEE International Conference on Communications*, volume 3, pages 1775–1779. IEEE, 1993.

[35] Daniel W Bliss, Keith W Forsythe, Alfred O Hero, and Ali F Yegulalp. Environmental issues for mimo capacity. *IEEE Transactions on Signal Processing*, 50(9):2128–2142, 2002.

[36] Emre Telatar. Capacity of multi-antenna gaussian channels. *European transactions on telecommunications*, 10(6):585–595, 1999.

[37] Arogyaswami Paulraj, Arogyaswami Paulraj Rohit, Rohit Nabar, and Dhananjay Gore. *Introduction to space-time wireless communications*. Cambridge university press, 2003.

[38] Thomas L Marzetta and Hien Quoc Ngo. *Fundamentals of massive MIMO*. Cambridge University Press, 2016.

[39] Thomas L Marzetta. Massive mimo: an introduction. *Bell Labs Technical Journal*, 20:11–22, 2015.

[40] Thomas L Marzetta. Blast training: Estimating channel characteristics for high capacity space-time wireless. In *Proceedings of the Annual Allerton Conference on Communication Control and Computing*, volume 37, pages 958–966. Citeseer, 1999.

[41] Hien Quoc Ngo, Erik G. Larsson, and Thomas L. Marzetta. Massive mu-mimo downlink tdd systems with linear precoding and downlink pilots. In *2013 51st Annual Allerton Conference on Communication, Control, and Computing (Allerton)*, pages 293–298, 2013.

[42] Erik G Larsson, Ove Edfors, Fredrik Tufvesson, and Thomas L Marzetta. Massive mimo for next generation wireless systems. *IEEE communications magazine*, 52(2):186–195, 2014.

[43] Thomas L Marzetta and Bertrand M Hochwald. Fast transfer of channel state information in wireless systems. *IEEE Transactions on Signal Processing*, 54(4):1268–1278, 2006.

[44] Thomas L. Marzetta. Noncooperative cellular wireless with unlimited numbers of base station antennas. *IEEE Transactions on Wireless Communications*, 9(11):3590–3600, 2010.

[45] Thomas L Marzetta and Alexei Ashikhmin. Mimo system having a plurality of service antennas for data transmission thereof, November 26 2013. US Patent 8,594,215.

[46] Fredrik Rusek, Daniel Persson, Buon Kiong Lau, Erik G Larsson, Thomas L Marzetta, Ove Edfors, and Fredrik Tufvesson. Scaling up mimo: Opportunities and challenges with very large arrays. *IEEE signal processing magazine*, 30(1):40–60, 2012.

[47] Hien Quoc Ngo, Alexei Ashikhmin, Hong Yang, Erik G Larsson, and Thomas L Marzetta. Cell-free massive mimo versus small cells. *IEEE Transactions on Wireless Communications*, 16(3):1834–1850, 2017.

[48] Emil Björnson and Luca Sanguinetti. Making cell-free massive mimo competitive with mmse processing and centralized implementation. *IEEE Transactions on Wireless Communications*, 19(1):77–90, 2019.

[49] Jiayi Zhang, Shuaifei Chen, Yan Lin, Jiakang Zheng, Bo Ai, and Lajos Hanzo. Cell-free massive mimo: A new next-generation paradigm. *IEEE Access*, 7:99878–99888, 2019.

[50] Long D Nguyen, Trung Q Duong, Hien Quoc Ngo, and Kamel Tourki. Energy efficiency in cell-free massive mimo with zero-forcing precoding design. *IEEE Communications Letters*, 21(8):1871–1874, 2017.

[51] Andreia Pereira, Fredrik Rusek, Marco Gomes, and Rui Dinis. Deployment strategies for large intelligent surfaces. *IEEE Access*, 10:61753–61768, 2022.

[52] Hien Quoc Ngo, Le-Nam Tran, Trung Q Duong, Michail Matthaiou, and Erik G Larsson. On the total energy efficiency of cell-free massive mimo. *IEEE Transactions on Green Communications and Networking*, 2(1):25–39, 2017.

[53] Filipe Conceição, Carlos Henggeler Antunes, Marco Gomes, Vitor Silva, and Rui Dinis. Max-min fairness optimization in uplink cell-free massive mimo using meta-heuristics. *IEEE Transactions on Communications*, 70(3):1792–1807, 2022.

[54] Zheng Chen and Emil Björnson. Channel hardening and favorable propagation in cell-free massive mimo with stochastic geometry. *IEEE Transactions on Communications*, 66(11):5205–5219, 2018.

[55] Ibrahim A. Hemadeh, Katla Satyanarayana, Mohammed El-Hajjar, and Lajos Hanzo. Millimeter-wave communications: Physical channel models, design considerations, antenna constructions, and link-budget. *IEEE Communications Surveys Tutorials*, 20(2):870–913, 2018.

[56] Giovanni Interdonato, Emil Björnson, Hien Quoc Ngo, Pål Frenger, and Erik G Larsson. Ubiquitous cell-free massive mimo communications. *EURASIP Journal on Wireless Communications and Networking*, 2019(1):1–13, 2019.

[57] Stefano Buzzi and Carmen D'Andrea. Cell-free massive mimo: User-centric approach. *IEEE Wireless Communications Letters*, 6(6):706–709, 2017.

[58] Sha Hu, Fredrik Rusek, and Ove Edfors. Beyond massive mimo: The potential of data transmission with large intelligent surfaces. *IEEE Transactions on Signal Processing*, 66(10):2746–2758, 2018.

[59] Robin Jess Williams, Elisabeth De Carvalho, and Thomas L Marzetta. A communication model for large intelligent surfaces. In *2020 IEEE International Conference on Communications Workshops (ICC Workshops)*, pages 1–6. IEEE, 2020.

Appendix A

Channel Model Derivations

Here we present details of mathematical derivations of the results presented in chapter 4.

A.1 Radio Stripe Array Gain Coefficient

As explained in chapter 4, for a single-user case, the array gain obtained through the coherent combination of the received signals throughout all the Radio Stripe (RS), is expressed by ϕ. As the RS was modeled as a continuous of antennas, the signal processing is done through an integral. Therefore, the coefficient ϕ is given by

$$\phi = \int_a^b \frac{D}{4\pi d^3}\, dx = \int_a^b \frac{D}{4\pi \left(D^2 + x^2\right)^{3/2}}\, dx = \frac{D}{4\pi}\int_a^b \frac{1}{\left(D^2 + x^2\right)^{3/2}}\, dx\,, \tag{A.1}$$

Assuming that $\{D, x\} \in \mathbb{R}$, then a substitution of the integrand variable can be made such that $x = D\tan(u)$ and $dx = D\sec^2(u)\, du$, with respective $u = \tan^{-1}(x/D)$ and $du = [D\sec^2(x)]^{-1}\, dx$.

Applying this substitution together with the trigonometrical identity $\tan(\theta) = \sqrt{\sec^2(\theta) + 1}$, we obtain

$$\left[D^2 + x^2\right]^{3/2} = \left[D^2 + (D\tan(u))^2\right]^{3/2} = \left[D^2 + D^2 \cdot (\sec^2(u) - 1)\right]^{3/2} = D^3\sec^3(u)\,. \tag{A.2}$$

Following that, the indefinite integral becomes

$$\frac{D}{4\pi}\int \frac{D\sec^2(u)}{D^3\sec^3(u)}\, du = \frac{1}{4\pi D}\int \frac{1}{\sec(u)}\, du = \frac{1}{4\pi D}\int \cos(u)\, du = \frac{\sin(u)}{4\pi D}\,. \tag{A.3}$$

Substituting back for $u = \tan^{-1}(x/D)$ returns

$$\int \frac{D}{4\pi \left(D^2 + x^2\right)^{3/2}}\, dx = \frac{\sin(\tan^{-1}(x/D)}{4\pi D} = \frac{x}{4\pi D\sqrt{x^2 + D^2}}\,, \tag{A.4}$$

by simplifying $\sin(\tan^{-1}(z) = z/\sqrt{z^2 + 1}$.

For an infinite RS, the integral in (A.1), is defined in the interval $[-\infty, \infty]$, therefore the resulting array gain coefficient is

$$\phi_{inf} = \left[\frac{x}{4\pi D\sqrt{x^2+D^2}}\right]\Bigg|_{x=\infty} - \left[\frac{x}{4\pi D\sqrt{x^2+D^2}}\right]\Bigg|_{x=-\infty} = \frac{1}{4\pi D} - \left[-\frac{1}{4\pi D}\right] = \frac{1}{2\pi D}\,, \quad \text{(A.5)}$$

while for RS with limited length L, the array gain for a User Equipment (UE) positioned at a position $(x, y) = (X, D)$, is

$$\begin{aligned}\phi_{limited} &= \left[\frac{x}{4\pi D\sqrt{x^2+D^2}}\right]\Bigg|_{x=L/2-X} - \left[\frac{x}{4\pi D\sqrt{x^2+D^2}}\right]\Bigg|_{x=-L/2-X} \\ &= \frac{1}{4\pi D}\left(\frac{\frac{L}{2}-X}{\sqrt{D^2+(\frac{L}{2}-X)^2}} - \frac{-\frac{L}{2}-X}{\sqrt{D^2+(-\frac{L}{2}-X)^2}}\right).\end{aligned} \quad \text{(A.6)}$$

For a centered UE, i.e. $(x, y) = (0, D)$, then

$$\phi_{limited} = \frac{1}{2\pi D}\frac{L}{(4D^2+L^2)^{1/2}}\,. \quad \text{(A.7)}$$